

Hamiltonian Particle-in-Cell methods for Vlasov–Poisson equations

Anjiao Gu^{a,b}, Yang He^c, Yajuan Sun^{a,b,*}

^aLSEC, ICMSEC, Academy of Mathematics and Systems Science, Chinese Academy of Sciences, Beijing 100190, China

^bSchool of Mathematical Sciences, University of Chinese Academy of Sciences, Beijing 100049, China

^cSchool of Mathematics and Physics, University of Science and Technology Beijing, Beijing 100083, China

Abstract

In this paper, Particle-in-Cell algorithms for the Vlasov–Poisson system are presented based on its Poisson bracket structure. The Poisson equation is solved by finite element methods, in which the appropriate finite element spaces are taken to guarantee that the semi-discretized system possesses a well defined discrete Poisson bracket structure. Then, splitting methods are applied to the semi-discretized system by decomposing the Hamiltonian function. The resulting discretizations are proved to be Poisson bracket preserving. Moreover, the conservative quantities of the system are also well preserved. In numerical experiments, we use the presented numerical methods to simulate various physical phenomena. Due to the huge computational effort of the practical computations, we employ the strategy of parallel computing. The numerical results verify the efficiency of the new derived numerical discretizations.

Keywords: Vlasov–Poisson system, Poisson bracket, Finite element method, Structure-preserving algorithm, Hamiltonian splitting method

1. Introduction

The motion of charged particles under electromagnetic fields is the most fundamental physical process in magnetized plasma. If only one particle is concerned, the dynamics can be described by the single particle model. If we are researching the interactive dynamics of a large number of particles with self-consistent electromagnetic fields, the kinetic model can be applied. In this model the Vlasov equation is applied together with the Maxwell equations or the Poisson equation, and the coupled system is called the Vlasov–Maxwell (VM) system or Vlasov–Poisson (VP) system respectively.

There are two main classes of numerical methods to solve the Vlasov type equations, the Eulerian method and the particle method. The Eulerian method, also called the grid-based method, is to discretize the PDEs model on fixed computational grid, and to carry out the time integration of the distribution function on mesh points. Various Eulerian approaches such as finite element methods, finite volume methods and spectral methods etc. have been developed

*Corresponding author at: LSEC, ICMSEC, Academy of Mathematics and Systems Science, Chinese Academy of Sciences, Beijing 100190, China; School of Mathematical Sciences, University of Chinese Academy of Sciences, Beijing 100049, China.

Email address: sunyj@lsec.cc.ac.cn (Yajuan Sun)

and applied to the plasma problems, see [24, 47, 56] and references therein. Different from the grid-based method the Particle-in-Cell (PIC) approach is to approximate the distribution function by ‘super particles’ with the weighted Klimontovich representation, and to follow the trajectories of super particles. Indeed, PIC has a relatively small computational cost to conduct high dimensional simulations [16, 38]. Although the introduction of super particles brings computational noise, it has been confirmed that the computational noise will decrease in the rate of $1/\sqrt{N_p}$ along the increasing number N_p of particles. The numerical simulation using the PIC technique can reproduce well the realistic physical phenomena [34, 5], and has been considered as an effective way to simulate plasmas of the kinetic theory [13].

In most applications, there span a wide range of space and time scales for the problem, which demands numerical simulations over large time intervals. Classical numerical methods, such as RK4, can approximate the solution well in the first few number of iterations. However, the numerical error accumulates rapidly over steps, and usually leads to wrong numerical results after a large number of iterations [20]. One reason is that these methods can not preserve the important conservative quantities of the original system. Structure-preserving algorithms (or geometric numerical integrators) are designed to conserve the intrinsic properties of the original system, including the symplectic structure, the Poisson structure, the invariant phase space volume, and constants of motions etc.. As a result the long-term stability of the numerical results can be guaranteed [19, 29, 21]. In [33, 32], the K -symplectic algorithms and the volume-preserving algorithms have been developed for solving the single particle equations. These numerical algorithms provide the numerical simulations with bounded energy error, and the trajectories of particles are well simulated over exponentially long simulation time.

It is known that the Vlasov–Maxwell system can be written as a Hamiltonian system with respect to the Morrison–Marsden–Weinstein (MMW) Poisson bracket [45, 41]. The Vlasov–Poisson system can be taken as the reduced Vlasov–Maxwell system. In this paper, we study the Poisson bracket structure of the Vlasov–Poisson system, and verify that the Poisson bracket of the Vlasov–Poisson system has very closed relation to the MMW Poisson bracket. As the Poisson bracket is usually not canonical, conventional time integrators are not structure-preserving. However, the splitting technique [58, 42] can be applied. High-order Hamiltonian splitting methods have been developed for Vlasov–Maxwell equations [57, 52, 31, 36, 38] and Vlasov–Poisson equations without magnetic fields [14, 8]. Correspondingly, spatial discretizations should also be designed carefully to maintain the structure. For the VM system, with the help of specially designed finite element spaces, the researchers [31, 36, 7] provide the semi-discrete system which can conserve the discrete Poisson structure corresponding to the original one. In other ways, a discrete Poisson bracket can also be obtained by applying discrete exterior calculus [57, 52, 36] and the variational principle [55, 18, 51]. On the other hand, in simulations of magnetic confinement fusion, Vlasov equation with a strong non-homogeneous magnetic field has aroused wide interest recently. Asymptotic preserving techniques [35, 59, 22, 28] and uniformly accurate schemes [3, 9] are efficient and characteristic numerical methods for them.

In this paper, we have developed the Hamiltonian Particle-in-Cell methods for the VP system with an external magnetic field. We first derive particle equations from the discretisation of the Vlasov equation, then the Poisson

equation is solved by finite element methods, with the finite element spaces chosen such that the semi-discrete system is Hamiltonian with a discrete Poisson structure. Furthermore, the Hamiltonian of the semi-discrete system is split into two parts, each of which possesses the same Poisson structure and can be solved exactly. By composing the solutions to the subsystems results in the Poisson-structure-preserving discretizations for the semi-discrete equations. In the numerical simulations, the parallel technique has been employed, and the effectiveness of the resulting numerical discretizations has been tested in numerical experiments.

The outline of the paper is as follows. In section 2, we introduce the various descriptions for the Vlasov equation. For the VP equation, in section 3 we present the Hamiltonian formulation which is described with the defined Poisson bracket structure. Furthermore, we apply the finite element methods to construct the numerical methods for VP system in Section 4. The corresponding discrete Poisson bracket and the discrete Hamiltonian are also established in this section. In Section 5, we split the Hamiltonian in order to construct the numerical discretizations which can preserve the discrete Poisson bracket. We display the numerical results in Section 6. Finally, we conclude this paper.

2. Equations

In the kinetic model, the Vlasov equation is in the form

$$\frac{\partial f}{\partial t} + \mathbf{v} \cdot \frac{\partial f}{\partial \mathbf{x}} + \frac{\mathbf{F}(\mathbf{x}, \mathbf{v}, t)}{m} \cdot \frac{\partial f}{\partial \mathbf{v}} = 0,$$

where $f(\mathbf{x}, \mathbf{v}, t)$ is the distribution function of position $\mathbf{x} \in \Omega_x \subset \mathbb{R}^3$ and velocity $\mathbf{v} \in \Omega_v \subset \mathbb{R}^3$ at time t , and \mathbf{F} is the force field acting on the particles. In most cases, the charged particles are considered to interact with the self-consistent electromagnetic fields in vacuum. This yields the following Maxwell's equations,

$$\begin{aligned} \mu_0 \epsilon_0 \frac{\partial \mathbf{E}}{\partial t} &= \nabla \times \mathbf{B} - \mu_0 q \int_{\Omega_v} \mathbf{v} f d\mathbf{v}, \quad \nabla \cdot \mathbf{B} = 0, \\ \frac{\partial \mathbf{B}}{\partial t} &= -\nabla \times \mathbf{E}, \quad \epsilon_0 \nabla \cdot \mathbf{E} = q \int_{\Omega_v} f d\mathbf{v} - q \rho_0, \end{aligned}$$

where μ_0 is the magnetic permeability, ϵ_0 is the vacuum permittivity and the constant ρ_0 is the charge density of ions. Then the force is given by $\mathbf{F} = q(\mathbf{E} + \mathbf{v} \times \mathbf{B})$ with q the charge. Choose the characteristic set of variables as they are shown in Table 1. Set $\bar{v} = c$, we can derive the normalized equations,

$$\begin{aligned} \frac{\partial f}{\partial t} + \mathbf{v} \cdot \frac{\partial f}{\partial \mathbf{x}} + (\mathbf{E} + \mathbf{v} \times \mathbf{B}) \cdot \frac{\partial f}{\partial \mathbf{v}} &= 0, \\ \frac{\partial \mathbf{E}}{\partial t} &= \nabla \times \mathbf{B} - \int_{\Omega_v} \mathbf{v} f d\mathbf{v}, \quad \nabla \cdot \mathbf{B} = 0, \\ \frac{\partial \mathbf{B}}{\partial t} &= -\nabla \times \mathbf{E}, \quad \nabla \cdot \mathbf{E} = \int_{\Omega_v} f d\mathbf{v} - \rho_0. \end{aligned} \tag{1}$$

In the magnetostatic limit, i.e. the case of $\frac{\partial \mathbf{B}}{\partial t} \rightarrow 0$, the magnetic field can be taken as a background field. Denote the background magnetic field as $\mathbf{B} = \mathbf{B}_0(\mathbf{x})$, the charge density as $\rho(\mathbf{x}, t) = \int_{\Omega_v} f d\mathbf{v}$ and the current density as

Names	Symbols	Units
Time	t	$1/\omega_p$
Position	x	λ
Velocity	v	\bar{v}
Distribution function	f	n_0/\bar{v}^3
Electric field	E	$\omega_p \bar{v} \frac{m}{q}$
Magnetic field	B	$\omega_p \frac{m}{q}$

Table 1: Units of Normalization. Here, \bar{v} is the characteristic scale of v , $\omega_p = \sqrt{n_0 q^2 / m \epsilon_0}$ is the electron plasma frequency with total number of electrons by $n_0 = \int_{\Omega_x \times \Omega_v} f dx dv$, and $\lambda = \bar{v} / \omega_p$.

$\mathbf{J}(\mathbf{x}, t) = \int_{\Omega_v} \mathbf{v} f d\mathbf{v}$. The VM system (1) is reduced to

$$\frac{\partial f}{\partial t} + \mathbf{v} \cdot \frac{\partial f}{\partial \mathbf{x}} + (\mathbf{E} + \mathbf{v} \times \mathbf{B}_0) \cdot \frac{\partial f}{\partial \mathbf{v}} = 0, \quad (2)$$

$$\frac{\partial \mathbf{E}}{\partial t} = \nabla \times \mathbf{B}_0 - \mathbf{J}, \quad \nabla \cdot \mathbf{B}_0 = 0, \quad (3)$$

$$\nabla \times \mathbf{E} = 0, \quad \nabla \cdot \mathbf{E} = \rho - \rho_0. \quad (4)$$

The total charge neutrality of the reduced system is ensured due to $\int_{\Omega_x} (\rho - \rho_0) d\mathbf{x} = 0$.

Notice that Maxwell's equations (3) and (4) can be decoupled, thus the system can be treated in two different ways. The first way is to consider Ampère's equation,

$$\frac{\partial \mathbf{E}}{\partial t} = \nabla \times \mathbf{B}_0 - \mathbf{J}. \quad (5)$$

It together with Eq.(2) is called the Vlasov–Ampère equation [17, 10, 11, 49].

Another way is to consider Faraday's law and Gauss's equation,

$$\nabla \times \mathbf{E} = 0, \quad \nabla \cdot \mathbf{E} = \rho - \rho_0.$$

By introducing the electric potential ϕ_f , it follows that

$$\mathbf{E}(\mathbf{x}, t) = -\nabla \phi_f(\mathbf{x}, t), \quad -\Delta \phi_f = \rho(\mathbf{x}, t) - \rho_0. \quad (6)$$

Combining Eqs.(2) and (6) derives the so-called Vlasov–Poisson equations.

As above, we have introduced two different reduced equations: the Vlasov–Poisson equation (2,6) and the Vlasov–Ampère equation (2,5). Moreover, the two equations are connected. By taking the divergence and curl of Ampère's equation (5), Eqs.(4) can be derived under the continuity condition $\frac{\partial \rho}{\partial t} + \nabla \cdot \mathbf{J} = 0$ and $\nabla \times \mathbf{J} = \Delta \mathbf{B}_0$, and the following restriction of the initial electric field,

$$\nabla \cdot \mathbf{E}(\mathbf{x}, 0) - \rho(\mathbf{x}, 0) + \rho_0 = 0, \quad \nabla \times \mathbf{E}(\mathbf{x}, 0) = 0.$$

Therefore, the solution of the Vlasov–Ampère equation under the above restrictions is a solution to the Vlasov–Poisson equation. In one dimensional case, in order to connect the solution of the Vlasov–Poisson equation to the solution of the Vlasov–Ampère equation [2], we can add the requirement $\int_{\Omega_x} E(x, t) dx = 0$ and the initial constraint $\int_{\Omega_x \times \Omega_v} v f(x, v, 0) dx dv = 0$.

In this paper, we mainly focus on the numerical study for the Vlasov–Poisson equations described by (2) and (6). In practical computation, the boundary conditions can be taken as zero, i.e., $f(\mathbf{x}, \mathbf{v}, t) = 0$ and $\phi_f(\mathbf{x}) = 0$ on $\partial\Omega_x$. Also the periodic boundary condition is used frequently.

3. Poisson bracket structure of Vlasov–Poisson equations

In this section, we introduce the Poisson bracket whose fundamental definition can be found in [48]. With the following defined Poisson bracket, in this section we describe the Vlasov–Poisson equations (2) and (6) as the Poisson bracket system.

Suppose \mathcal{F} and \mathcal{G} are two functionals of f , we define the bracket of two functionals as

$$\{\{\mathcal{F}, \mathcal{G}\}\}(f) = \int_{\Omega_x \times \Omega_v} f \left\{ \frac{\delta \mathcal{F}}{\delta f}, \frac{\delta \mathcal{G}}{\delta f} \right\}_{\mathbf{xv}} dx dv + \int_{\Omega_x \times \Omega_v} f \mathbf{B}_0 \cdot \left(\frac{\partial}{\partial \mathbf{v}} \frac{\delta \mathcal{F}}{\delta f} \times \frac{\partial}{\partial \mathbf{v}} \frac{\delta \mathcal{G}}{\delta f} \right) dx dv, \quad (7)$$

where $\frac{\delta \mathcal{G}}{\delta f}$ is the variational derivative¹, and the operator $\{\cdot, \cdot\}_{\mathbf{xv}}$ is the canonical Poisson bracket of two functions $m(\mathbf{x}, \mathbf{v})$ and $n(\mathbf{x}, \mathbf{v})$, that is

$$\{m, n\}_{\mathbf{xv}} = \frac{\partial m}{\partial \mathbf{x}} \cdot \frac{\partial n}{\partial \mathbf{v}} - \frac{\partial m}{\partial \mathbf{v}} \cdot \frac{\partial n}{\partial \mathbf{x}}.$$

It can be checked easily that the bracket (7) is bilinear and anti-symmetric. Furthermore, when \mathbf{B}_0 satisfies $\nabla \cdot \mathbf{B}_0(\mathbf{x}) = 0$, the bracket yields the Jacobi identity which has been proved in Appendix A.

With the bracket (7), we can present the following system,

$$\frac{d\mathcal{F}}{dt} = \{\{\mathcal{F}, \mathcal{H}\}\}, \quad (8)$$

where \mathcal{F} is any functional of the solution f , and \mathcal{H} is the Hamiltonian functional and the global energy of the system,

$$\begin{aligned} \mathcal{H}[f] &= \frac{1}{2} \int_{\Omega_x \times \Omega_v} \mathbf{v}^2 f dx dv + \frac{1}{2} \int_{\Omega_x} \mathbf{E}^2 dx \\ &= \frac{1}{2} \int_{\Omega_x \times \Omega_v} \mathbf{v}^2 f dx dv + \frac{1}{2} \int_{\Omega_x \times \Omega_v} \phi_f f dx dv - \frac{1}{2} \rho_0 \int_{\Omega_x} \phi_f dx. \end{aligned} \quad (9)$$

In fact, by setting $\mathcal{F}[f] = \int_{\Omega_x \times \Omega_v} f(\tilde{\mathbf{x}}, \tilde{\mathbf{v}}, t) \delta(\mathbf{x} - \tilde{\mathbf{x}}) \delta(\mathbf{v} - \tilde{\mathbf{v}}) d\tilde{\mathbf{x}} d\tilde{\mathbf{v}}$, and defining the local energy $h(\mathbf{x}, \mathbf{v}) = \frac{\delta \mathcal{H}}{\delta f}(\mathbf{x}, \mathbf{v}) = \mathbf{v}^2/2 + \phi_f(\mathbf{x})$, the formulation (8) leads to

$$\frac{\partial f}{\partial t} = -\{f, h\}_{\mathbf{xv}} - \mathbf{B}_0 \cdot \left(\frac{\partial f}{\partial \mathbf{v}} \times \frac{\partial h}{\partial \mathbf{v}} \right). \quad (10)$$

¹The variational derivative [46, 40] $\frac{\delta \mathcal{G}}{\delta f}$ of a functional $\mathcal{G}[f]$ is defined by

$$\int_{\Omega_x \times \Omega_v} \frac{\delta \mathcal{G}}{\delta f} \delta f dx dv = \lim_{\epsilon \rightarrow 0} \frac{\mathcal{G}[f + \epsilon \delta f] - \mathcal{G}[f]}{\epsilon}.$$

Eq. (10) recovers the Vlasov equation (2).

As a reduced model from the Vlasov–Maxwell equations, conservative properties of the Vlasov–Poisson system is also of great importance. With the help of the Poisson bracket (7) and the formulation (8), the conservative properties can be redescribed as follows.

Energy conservation. The total energy defined in (9) is invariant as

$$\frac{d\mathcal{H}}{dt} = \{\{\mathcal{H}, \mathcal{H}\}\} = 0.$$

Momentum conservation. The total momentum $\mathcal{P} = \int_{\Omega_x \times \Omega_v} \mathbf{v} f d\mathbf{x} d\mathbf{v}$ is invariant when $\mathbf{B}_0 = \mathbf{0}$.

In fact, taking the derivative of \mathcal{P} gives

$$\frac{d\mathcal{P}}{dt} = \{\{\mathcal{P}, \mathcal{H}\}\} = - \int_{\Omega_x} \nabla \phi_f \rho d\mathbf{x} + \int_{\Omega_x \times \Omega_v} (\mathbf{v} \times \mathbf{B}_0) f d\mathbf{x} d\mathbf{v}.$$

The first term vanishes due to the Poisson equation which is expressed as $\nabla \cdot \mathbf{E} = \rho - \rho_0$, $\nabla \times \mathbf{E} = \mathbf{0}$, because

$$\begin{aligned} - \int_{\Omega_x} \nabla \phi_f \rho d\mathbf{x} &= \int_{\Omega_x} \mathbf{E} (\nabla \cdot \mathbf{E} + \rho_0) d\mathbf{x} \\ &= - \int_{\Omega_x} (\nabla \times \mathbf{E}) \times \mathbf{E} d\mathbf{x} + \rho_0 \int_{\Omega_x} \mathbf{E} d\mathbf{x} = 0. \end{aligned}$$

Here, $\int_{\Omega_x} \mathbf{E} d\mathbf{x} = 0$ for zero or periodic boundary condition of ϕ_f .

Casimir functional. Any functional in the form $C[f] = \int_{\Omega_x \times \Omega_v} C(f) d\mathbf{x} d\mathbf{v}$ is invariant, as it is a Casimir functional [46] w.r.t the Poisson bracket (7) with $\mathbf{B}_0 = \mathbf{0}$. In fact, taking the bracket operation between $C[f]$ and any functional $\mathcal{G}[f]$ gives

$$\{\{C, \mathcal{G}\}\} = \int_{\Omega_x \times \Omega_v} \left\{ f, \frac{\delta C}{\delta f} \right\}_{\mathbf{x}\mathbf{v}} \frac{\delta \mathcal{G}}{\delta f} d\mathbf{x} d\mathbf{v}.$$

The above equation vanishes because $\frac{\delta C[f]}{\delta f} = C'(f)$ is a function of f . Therefore, $C[f]$ is an invariant for any PDE of f equipped with the Poisson bracket (7), including the Vlasov equation, that is

$$\frac{dC}{dt} = \{\{C, \mathcal{H}\}\} = 0.$$

This provides a class of conservative quantities of the Vlasov–Poisson system (2,6). For instance, the integral norm $I = \int_{\Omega_x \times \Omega_v} f^p d\mathbf{x} d\mathbf{v}$ and the entropy $S = \int_{\Omega_x \times \Omega_v} f \ln f d\mathbf{x} d\mathbf{v}$ of the system are invariant.

4. Spatial discretization for Vlasov–Poisson equations

In this section, we present the construction of numerical approach for solving the Vlasov–Poisson equations (2) and (6).

According to the idea of PIC, the distribution function is sampled by a set of super particles. Assume that the distribution function f is approximated by the Klimontovich representation

$$f_h(\mathbf{x}, \mathbf{v}, t) = \sum_{s=1}^{N_p} \omega_s \delta(\mathbf{x} - \mathbf{X}_s(t)) \delta(\mathbf{v} - \mathbf{V}_s(t)), \quad (11)$$

where $(\mathbf{X}_s, \mathbf{V}_s)$ is the s -th super particle's coordinates in phase space, and ω_s is the particle weight, N_p is the number of super particles. The Vlasov equation (2) is then transformed to particle equations,

$$\dot{\mathbf{X}}_s = \mathbf{V}_s, \quad \dot{\mathbf{V}}_s = \int_{\Omega_x} (\mathbf{E}(\mathbf{x}, t) + \mathbf{V}_s \times \mathbf{B}_0(\mathbf{x})) \delta(\mathbf{x} - \mathbf{X}_s) d\mathbf{x}, \quad s = 1, 2, \dots, N_p. \quad (12)$$

We use finite element methods to solve the Poisson equation (6) with the Dirichlet boundary condition, i.e.

$$-\Delta \phi_f = \rho - \rho_0 \text{ in } \Omega_x, \quad \phi_f(x, t) = 0 \text{ on } \partial\Omega_x.$$

Let V be a Hilbert space and V' be the dual space of it. In the framework of finite element, the variational problem of Poisson equation (6) is to find solutions $\phi \in V$ such that for any $\psi \in V$ the following equation holds

$$(\nabla \phi, \nabla \psi) = \langle \rho - \rho_0, \psi \rangle, \quad \forall \psi \in V. \quad (13)$$

Here, $\rho - \rho_0 \in V'$, (\cdot, \cdot) is the inner product of V and $\langle \cdot, \cdot \rangle$ is the pairing of elements of V' and V . It is known by the Lax-Milgram theorem that the solution to the variational problem (13) is unique [39, 6].

In order to determine the proper space V , we refer to [31, 36, 51] where finite element discretizations have been presented to derive Hamiltonian algorithms for the Vlasov–Maxwell equations. Given a linear operator $D \in \{\text{grad}, \text{curl}, \text{div}\}$, we denote the Sobolev spaces as

$$H(D, \Omega) := \{v \in L^2(\Omega), Dv \in L^2(\Omega)\},$$

$$H_0(D, \Omega) := \{v \in H(D, \Omega), \text{trace } v = 0 \text{ on } \partial\Omega\}.$$

Denote $H^h(D, \Omega)$ as the finite element subspace of $H(D, \Omega)$. For the finite element PIC discretisation of the Vlasov–Maxwell equations (1), we have the following results. Here the perfect conducting boundary (PEC) conditions are considered.

Proposition 1 ([31]). *Suppose that the fields \mathbf{E} and \mathbf{B} are discretised in spaces $\mathcal{E}_h \subset H_0(\text{curl}, \Omega)$ and $\mathcal{B}_h \subset H_0(\text{div}, \Omega)$ respectively. The approximate problem for Maxwell's equations is to find $(\mathbf{E}_h, \mathbf{B}_h) \in \mathcal{E}_h \times \mathcal{B}_h$ such that*

$$\begin{aligned} (\partial_t \mathbf{E}_h, \Phi) &= (\mathbf{B}_h, \nabla \times \Phi) - \left(\sum_s \omega_s \mathbf{V}_s \delta(\mathbf{x} - \mathbf{X}_s), \Phi \right), \quad \forall \Phi \in \mathcal{E}_h, \\ (\partial_t \mathbf{B}_h, \Psi) &= -(\nabla \times \mathbf{E}_h, \Psi), \quad \forall \Psi \in \mathcal{B}_h. \end{aligned}$$

If $\nabla \times \mathcal{E}_h \subset \mathcal{B}_h$ and $\nabla \cdot \mathbf{B}_h = 0$, the resulting semi-discrete system is Hamiltonian with a discrete Poisson structure.

To understand the above theorem, we can employ the following diagram. That is, in order to derive a discrete Hamiltonian system, we need choose the finite element to satisfies the de Rham Complex diagram

$$\begin{array}{ccccccc} H(\text{grad}) & \xrightarrow{\text{grad}} & H(\text{curl}) & \xrightarrow{\text{curl}} & H(\text{div}) & \xrightarrow{\text{div}} & L^2 \\ \pi \downarrow & & \pi \downarrow & & \pi \downarrow & & \pi \downarrow \\ H^h(\text{grad}) & \xrightarrow{\text{grad}} & H^h(\text{curl}) & \xrightarrow{\text{curl}} & H^h(\text{div}) & \xrightarrow{\text{div}} & L^{2,h} \end{array}$$

According to the above comment and the relation $\mathbf{E} = -\nabla\phi$, for $\mathbf{E} \in H_0(\text{curl}, \Omega)$ we can choose $\phi \in V = H_0(\text{grad}, \Omega_x)$.

The approximate problem of (13) is then to find $\phi_h \in V_h \subset H_0^1(\Omega_x)$ such that

$$(\nabla\phi_h, \nabla\psi_h) = \langle \rho_h, \psi_h \rangle, \quad \forall \psi_h \in V_h. \quad (14)$$

Here, $\rho_h \in L^2(\Omega_x)$ is the discrete version of $\rho - \rho_0$. The inner product is defined by $(\mathbf{f}, \mathbf{g}) = \int_{\Omega_x} \mathbf{f} \cdot \mathbf{g} d\mathbf{x}$ on space $L^2(\Omega_x)$ and V_h is the finite-dimensional subspace. In particular, for all $\psi_h \in H_0^1(\Omega_x)$ and $\rho_h \in L^2(\Omega_x) \subset H^{-1}(\Omega_x)$, we have $(\rho_h, \psi_h) = \langle \rho_h, \psi_h \rangle$, and the solution to the variational problem (14) is unique. Thus, the well studied finite element spaces including linear element, quadratic Lagrange element, and Spline element etc. can be implemented.

Suppose that $\{W_j(\mathbf{x})\}_{j=1}^N$ are piecewise polynomial basis functions of the space V_h , then $\phi_h \in V_h$ can be expressed as

$$\phi_h(\mathbf{x}, t) = \sum_{j=1}^N \phi_j(t) W_j(\mathbf{x}). \quad (15)$$

In order to get an appropriate regularization of ρ_h , we introduce the regularizing function $S_\epsilon(\mathbf{x})$ which satisfies $\int_{\mathbb{R}^d} S(\mathbf{x}) d\mathbf{x} = 1$ and $S_\epsilon(\mathbf{x}) = \frac{1}{\epsilon^d} S(\frac{\mathbf{x}}{\epsilon})$ [53, 12, 27]. Here ϵ denotes the width of the kernel and $d = 1, 2, 3$.

Then, we define $f_h^\epsilon = f_h * S_\epsilon$, that is $f_h^\epsilon(\mathbf{x}, \mathbf{v}, t) = \sum_{s=1}^{N_p} \omega_s S_\epsilon(\mathbf{x} - \mathbf{X}_s(t)) \delta(\mathbf{v} - \mathbf{V}_s(t))$. By means of S_ϵ , we can choose $\rho_h(\mathbf{x}) = \sum_{s=1}^{N_p} \omega_s S_\epsilon(\mathbf{x} - \mathbf{X}_s) - \rho_0$ derived from $\rho_h(\mathbf{x}, t) = \int_{\Omega_v} f_h^\epsilon(\mathbf{x}, \mathbf{v}, t) d\mathbf{v} - \rho_0$. On the other hand, ρ_h can be projected to the space V_h , which gives $\rho_h(\mathbf{x}) = \sum_{i=1}^N \rho_i W_i(\mathbf{x})$. This will help us in computation due to that (W_i, W_j) can be calculated easily, and $\rho_h \in V_h \subset H_0^1 \subset L^2$.

Substitute Eq.(15) into Eq.(14) and take $\psi_h = W_i$, then we get the following approximate problem in matrix formulation,

$$\sum_{j=1}^N (\nabla W_j, \nabla W_i) \phi_j = (\rho_h, W_i), \quad i = 1 \dots N, \quad (16)$$

where the solutions $\{\phi_j\}_{j=1}^N$ are the functions of particle positions \mathbf{X}_s , $s = 1, 2, \dots, N_p$. In order to get a vector expression for the particles, we denote $\mathbf{X} = (\mathbf{X}_1^T, \mathbf{X}_2^T, \dots, \mathbf{X}_{N_p}^T)^T \in \mathbb{R}^{3N_p}$ and $\mathbf{V} = (\mathbf{V}_1^T, \mathbf{V}_2^T, \dots, \mathbf{V}_{N_p}^T)^T \in \mathbb{R}^{3N_p}$. Then the approximate electric field is

$$\mathbf{E}_h(\mathbf{x}, \mathbf{X}, t) = - \sum_{j=1}^N \phi_j(\mathbf{X}(t)) \nabla W_j(\mathbf{x}). \quad (17)$$

Substituting \mathbf{E}_h into Eq. (12), we get the discrete particle equations for $s = 1, 2, \dots, N_p$,

$$\begin{aligned} \dot{\mathbf{X}}_s &= \mathbf{V}_s, \\ \dot{\mathbf{V}}_s &= - \sum_{j=1}^N \phi_j(\mathbf{X}) \nabla W_j(\mathbf{X}_s) + \mathbf{V}_s \times \mathbf{B}_0(\mathbf{X}_s). \end{aligned} \quad (18)$$

Define the discrete bracket by discretizing the Poisson bracket (7) shown in Appendix B. Moreover, it is proved in Appendix C that the following discrete bracket is Poisson as long as $\nabla \cdot \mathbf{B}_0(\mathbf{x}) = 0$. With the defined discrete Poisson

bracket, the semi-discrete system (18) is a Hamiltonian ODE system. For two arbitrary functions F and G of (\mathbf{X}, \mathbf{V}) , it reads

$$\{F, G\}(\mathbf{X}, \mathbf{V}) = \sum_{s=1}^{N_p} \frac{1}{\omega_s} \left(\frac{\partial F}{\partial \mathbf{X}_s} \cdot \frac{\partial G}{\partial \mathbf{V}_s} - \frac{\partial G}{\partial \mathbf{X}_s} \cdot \frac{\partial F}{\partial \mathbf{V}_s} \right) + \sum_{s=1}^{N_p} \frac{1}{\omega_s} \mathbf{B}_0(\mathbf{X}_s) \cdot \left(\frac{\partial F}{\partial \mathbf{V}_s} \times \frac{\partial G}{\partial \mathbf{V}_s} \right). \quad (19)$$

Accordingly, by inserting (11) into (9) we can derive the following discrete Hamiltonian function,

$$\begin{aligned} H(\mathbf{X}, \mathbf{V}) &= \mathcal{H}[f_h] = \frac{1}{2} \int_{\Omega_x \times \Omega_v} \mathbf{v}^2 f_h d\mathbf{x} d\mathbf{v} + \frac{1}{2} \int_{\Omega_x} (\nabla \phi_h) \cdot (\nabla \phi_h) d\mathbf{x} \\ &= \frac{1}{2} \sum_{s=1}^{N_p} \omega_s \mathbf{V}_s^2 + \frac{1}{2} \sum_{j=1}^N \sum_{k=1}^N \phi_j(\mathbf{X}) \phi_k(\mathbf{X}) \int_{\Omega_x} \nabla W_j(\mathbf{x}) \cdot \nabla W_k(\mathbf{x}) d\mathbf{x} \end{aligned} \quad (20)$$

For the finite element discretization, the discrete Hamiltonian function (20) is natural, and can be rewritten in matrix form easily. With the discrete Poisson bracket (19) and the discrete Hamiltonian (20), the semi-discrete equations of motion (18) can be recovered by

$$\dot{\mathbf{X}}_s = \{\mathbf{X}_s, H\}, \quad \dot{\mathbf{V}}_s = \{\mathbf{V}_s, H\}. \quad (21)$$

As follows, we express the semi-discretised equations (21) by their matrix formulation. Introduce the following notations for the field basis and variables:

$$\begin{aligned} \Phi(\mathbf{X}) &= (\phi_1, \phi_2, \dots, \phi_N)^T(\mathbf{X}) \in \mathbb{R}^N, \quad \mathbb{M} \in \mathbb{R}^{N \times N}, \quad \text{with } \mathbb{M}_{jk} = \int_{\Omega_x} \nabla W_j(\mathbf{x}) \cdot \nabla W_k(\mathbf{x}) d\mathbf{x}, \\ \mathbb{G}(\mathbf{X}) &= \begin{pmatrix} \nabla W_1(\mathbf{X}_1) & \nabla W_2(\mathbf{X}_1) & \cdots & \nabla W_N(\mathbf{X}_1) \\ \nabla W_1(\mathbf{X}_2) & \nabla W_2(\mathbf{X}_2) & \cdots & \nabla W_N(\mathbf{X}_2) \\ \cdots & \cdots & \cdots & \cdots \\ \nabla W_1(\mathbf{X}_{N_p}) & \nabla W_2(\mathbf{X}_{N_p}) & \cdots & \nabla W_N(\mathbf{X}_{N_p}) \end{pmatrix} \in \mathbb{R}^{(3N_p) \times N}, \\ \hat{\mathbb{B}}(\mathbf{X}) &= \text{diag}(\hat{\mathbf{B}}_0(\mathbf{X}_1), \hat{\mathbf{B}}_0(\mathbf{X}_2), \dots, \hat{\mathbf{B}}_0(\mathbf{X}_{N_p})) \in \mathbb{R}^{(3N_p) \times (3N_p)}. \end{aligned}$$

where $\hat{\mathbf{B}}_0$ is the hat matrix w.r.t the vector \mathbf{B}_0 . The hat matrix of a vector $\mathbf{B} = (B_x, B_y, B_z)$ is defined as

$$\hat{\mathbf{B}} = \begin{pmatrix} 0 & B_z & -B_y \\ -B_z & 0 & B_x \\ B_y & -B_x & 0 \end{pmatrix}. \quad (22)$$

Denote the diagonal weight matrix $\mathbf{\Omega} = \text{diag}(\omega_1, \omega_2, \dots, \omega_{N_p}) \in \mathbb{R}^{N_p \times N_p}$, and \mathbf{I} as the 3-dimensional identity matrix.

Let

$$\mathbb{N} = \mathbf{\Omega} \otimes \mathbf{I} \in \mathbb{R}^{(3N_p) \times (3N_p)}.$$

Therefore, the discrete Poisson bracket (19) can be reformulated in matrix form as

$$\begin{aligned} \{F, G\}(\mathbf{Z}) &= \sum_{s=1}^{N_p} \frac{1}{\omega_s} \left(\left(\frac{\partial F}{\partial \mathbf{X}_s} \right)^T, \left(\frac{\partial F}{\partial \mathbf{V}_s} \right)^T \right) \begin{pmatrix} 0 & \mathbf{I} \\ -\mathbf{I} & \hat{\mathbf{B}}_0(\mathbf{X}_s) \end{pmatrix} \begin{pmatrix} \frac{\partial G}{\partial \mathbf{X}_s} \\ \frac{\partial G}{\partial \mathbf{V}_s} \end{pmatrix} \\ &= \frac{\partial F^T}{\partial \mathbf{Z}} \mathbb{K}(\mathbf{X}) \frac{\partial G}{\partial \mathbf{Z}}, \end{aligned} \quad (23)$$

where $\mathbf{Z} = (\mathbf{X}, \mathbf{V})$, and $\mathbb{K}(\mathbf{X}) = \begin{pmatrix} 0 & \mathbb{N}^{-1} \\ -\mathbb{N}^{-1} & \mathbb{N}^{-1}\hat{\mathbb{B}}(\mathbf{X}) \end{pmatrix}$ is the Poisson matrix. With the above notations, the discrete Hamiltonian (20) can be rewritten as,

$$H(\mathbf{X}, \mathbf{V}) = \frac{1}{2}\mathbf{V}^T\mathbb{N}\mathbf{V} + \frac{1}{2}\boldsymbol{\Phi}(\mathbf{X})^T\mathbb{M}\boldsymbol{\Phi}(\mathbf{X}). \quad (24)$$

The corresponding system (18) can be rewritten with Poisson matrix $\mathbb{K}(\mathbf{X})$, which is

$$\begin{aligned} \dot{\mathbf{X}} &= \mathbf{V}, \\ \dot{\mathbf{V}} &= \mathbb{G}(\mathbf{X})\boldsymbol{\Phi}(\mathbf{X}) + \hat{\mathbb{B}}(\mathbf{X})\mathbf{V}. \end{aligned} \quad (25)$$

With the help of the discrete Poisson bracket, the conservation of the discrete energy $H(\mathbf{X}, \mathbf{V})$ in Eq.(20) can be easily verified, that is

$$\frac{dH}{dt} = \{H, H\}(\mathbf{X}, \mathbf{V}) = 0.$$

Similarly, the total charge $C = \int_{\Omega_x \times \Omega_v} f_h d\mathbf{x}d\mathbf{v} = \sum_{s=1}^{N_p} \omega_s$ is invariant, as it is a Casimir function of the discrete Poisson bracket (19),

$$\frac{dC}{dt} = \{C, H\}(\mathbf{X}, \mathbf{V}) \equiv 0.$$

5. Temporal discretization for Vlasov–Poisson equations

In this section we are designing temporal discretisation for the Vlasov–Poisson equations that can preserve the Poisson bracket structure. As the Poisson bracket is not canonical, traditional time integrators such as Runge-Kutta methods can not be used to construct Poisson-structure-preserving methods. The idea of splitting technique is to split the original system into several subsystems. Each subsystem can be solved exactly, and has the same structure as ones for the original system [58, 42]. Thus, the composition of solutions to subsystems leads to numerical methods which can preserve the structure of the original systems. High-order Hamiltonian splitting methods have been developed for Vlasov–Maxwell equations [30, 38] and Vlasov–Poisson equations without magnetic fields [14, 8]. In this section, for the non-canonical Hamiltonian ODE system (18) we establish the Poisson-structure-preserving methods via Hamiltonian splitting.

We split the Hamiltonian as,

$$H = H_v + H_e, \quad \text{where } H_v = \frac{1}{2} \sum_{s=1}^{N_p} \omega_s \mathbf{V}_s^2, \quad H_e = \frac{1}{2} \boldsymbol{\Phi}(\mathbf{X})^T \mathbb{M} \boldsymbol{\Phi}(\mathbf{X}).$$

With each part of the Hamiltonian, we can split the system into two parts,

$$\dot{\mathbf{Z}} = \{\mathbf{Z}, H_v\}, \quad \dot{\mathbf{Z}} = \{\mathbf{Z}, H_e\}.$$

Each subsystem possesses the same Poisson bracket structure as the system (18). Thus the composition of solutions to each subsystem preserves the Poisson bracket of the original system due the group property of Poisson bracket structure.

Associated with the Hamiltonian H_v , the subsystem is $\dot{F} = \{F, H_v\}$. For the s -th particle it is,

$$\begin{aligned}\dot{\mathbf{X}}_s &= \mathbf{V}_s, \\ \dot{\mathbf{V}}_s &= \mathbf{V}_s \times \mathbf{B}_0(\mathbf{X}_s).\end{aligned}\tag{26}$$

When \mathbf{B}_0 is constant and $|\mathbf{B}_0| = b$, the exact update mapping of this subsystem (26) with step size Δt is

$$\begin{aligned}\phi^{H_v}(\Delta t) : \\ \mathbf{X}_s(t + \Delta t) &= \mathbf{X}_s(t) + (\Delta t \mathbf{I} + \frac{1 - \cos b\Delta t}{b^2} \hat{\mathbf{B}}_0 + \frac{b\Delta t - \sin b\Delta t}{b^3} \hat{\mathbf{B}}_0^2) \mathbf{V}_s(t), \\ \mathbf{V}_s(t + \Delta t) &= (\mathbf{I} + \frac{\sin b\Delta t}{b} \hat{\mathbf{B}}_0 + \frac{1 - \cos b\Delta t}{b^2} \hat{\mathbf{B}}_0^2) \mathbf{V}_s(t).\end{aligned}\tag{27}$$

where $\hat{\mathbf{B}}_0$ is the hat matrix as in Eq.(22). Following the idea, we can also consider the problem in which \mathbf{B}_0 is non-homogeneous. In this case, we need to split the subsystem corresponding to H_v further according to its new decomposition $H_v = \frac{1}{2}\omega_s \mathbf{V}_{sx}^2 + \frac{1}{2}\omega_s \mathbf{V}_{sy}^2 + \frac{1}{2}\omega_s \mathbf{V}_{sz}^2$. More detail can be seen in [30].

The equation $\dot{F} = \{F, H_e\}$ associated with the Hamiltonian H_e is

$$\begin{aligned}\dot{\mathbf{X}}_s &= 0, \\ \dot{\mathbf{V}}_s &= - \sum_{j=1}^N \phi_j(\mathbf{X}(t)) \int_{\Omega_x} \nabla W_j(\mathbf{x}) \delta(\mathbf{x} - \mathbf{X}_s) d\mathbf{x}.\end{aligned}\tag{28}$$

The exact update of this subsystem (28) with step size Δt is

$$\begin{aligned}\mathbf{X}_s(t + \Delta t) &= \mathbf{X}_s(t), \\ \phi^{H_e}(\Delta t) : \\ \mathbf{V}_s(t + \Delta t) &= \mathbf{V}_s(t) - \Delta t \sum_{j=1}^N \phi_j(\mathbf{X}(t)) \int_{\Omega_x} \nabla W_j(\mathbf{x}) \delta(\mathbf{x} - \mathbf{X}_s) d\mathbf{x}.\end{aligned}\tag{29}$$

With the given exact solutions to the subsystems, Poisson integrators can be derived by the compositions of the sub-flows (27) and (29). For example, the Poisson method of first order can be constructed by

$$\Phi(\Delta t) = \phi^{H_e}(\Delta t) \circ \phi^{H_v}(\Delta t),$$

and a second order symmetric method can be derived from

$$\Phi(\Delta t) = \phi^{H_v}(\Delta t/2) \circ \phi^{H_e}(\Delta t) \circ \phi^{H_v}(\Delta t/2).$$

From the above, it is clear that these methods constructed by splitting can be implemented easily. More important, these methods can preserve the discrete Poisson bracket.

At the end of this section, we present the algorithm framework which helps to understand the computation procedure.

6. Numerical experiments

In this section, we present numerical experiments by using numerical methods presented in the previous section. The resulting numerical discretizations are derived by combining splitting method in time and finite element discretization in space. To derive the numerical results more efficiently we employ the parallel technique which is run on high performance computing workstation of LSEC Lab.

Algorithm 1 Algorithm framework

Input: $f(\mathbf{x}, \mathbf{v}, t = 0)$

- 1: Approximate the initial condition f_0 by the distribution $f_h^\epsilon(\mathbf{x}, \mathbf{v}, t = 0) = \sum_{s=1}^{N_p} \omega_s S_\epsilon(\mathbf{x} - \mathbf{X}_s(0)) \delta(\mathbf{v} - \mathbf{V}_s(0))$ where $(\mathbf{X}_s(0), \mathbf{V}_s(0))$ is a set of particles distributed in the phase space according to the density function f_0 .
- 2: Generate finite element mesh and assemble stiffness matrix \mathbb{M} .
- 3: Compute the density $\rho_h = \sum_{s=1}^{N_p} \omega_s S_\epsilon(\mathbf{x} - \mathbf{X}_s) - \rho_0$.
- 4: Assemble the load matrix F according to the density ρ_h . That is $F_i = (\rho_h, W_i)$, $i = 1 \dots N$.
- 5: Solve the large sparse linear system $\mathbb{M}\phi_h = F$. (A lot of linear solvers can be used such as Conjugate Gradient.)
- 6: Interpolate the electric field at the particle position by using discrete electric potential ϕ_h . We can just use the information of $\nabla W_i(\mathbf{x})$, $i = 1 \dots N$.
- 7: Update the position and velocity of particles by solving particle equation. High order symplectic algorithms can be considered.
- 8: Repeat steps 3-7 till the final time T .

Output: $f_h^\epsilon(\mathbf{x}, \mathbf{v}, t = T)$ or other required data

6.1. Test problems in 1+1-dimensional phase space

In this case, we perform various problems: Landau damping, Two-stream stability and Bump-on-tail instability. In the numerical simulation for all problems, we use periodic boundary condition. The number of particles is chosen as $N_p = 10^6$. The system considered here is modelled by Vlasov equation coupled with normalized Poisson equation

$$\mathbf{E} = -\partial\phi, \quad -\partial^2\phi = \rho - 1.$$

Landau damping. Landau damping is referred to as the damping of a collective mode of oscillations in plasmas without collisions of charged particles. It, commonly believed, is caused by the energy exchange between electromagnetic wave and particles. Landau damping is also a very popular benchmark problem for testing the numerical methods applied to the Vlasov–Poisson equation due to that there are many analytical results in literature [23, 16]. Here, we consider the case of one spatial dimension. In this case, we take the initial distribution function as

$$f_0(x, v) = \frac{1}{\sqrt{2\pi}} \exp\left(-\frac{v^2}{2}\right) (1 + \alpha \cos(kx)),$$

where the perturbation parameter $\alpha = 0.001$ and k is the wave number.

We use the time step $\Delta t = 0.01$. To solve the Poisson system we use $N_x = 128$. We choose the computation domain as $[0, 2\pi/k] \times [-6, 6]$. We are interested in the evolution of the square root of the electric energy which is measured by $E_d(t) = \sqrt{\Phi(\mathbf{X})^T \mathbb{M} \Phi(\mathbf{X})}$ with $\Phi(\mathbf{X})$ and \mathbb{M} mentioned in Section 4. In Figure 1, we calculate the value of $\log(E_d(t))$ along time t where the red line is the theoretical damping rate. It is observed that the electric energy is exponentially decreasing, and the damping rate coincides with the analytical values which are $\gamma = 0.0127$ for $k = 0.3$ and $\gamma = 0.154$ for $k = 0.5$ [25, 4, 16].

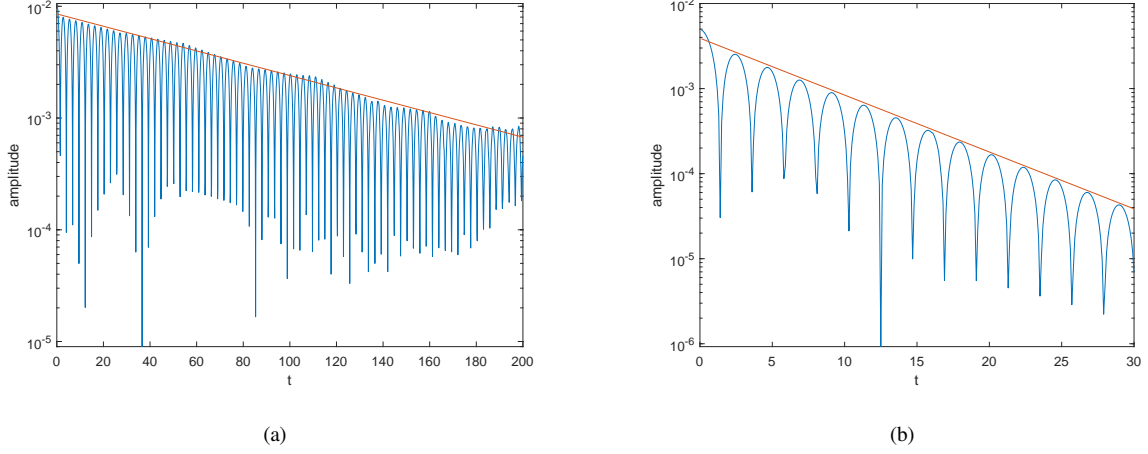


Figure 1: Electric energy as a function of time for the linear Landau damping. (a) $k = 0.3$; (b) $k = 0.5$.

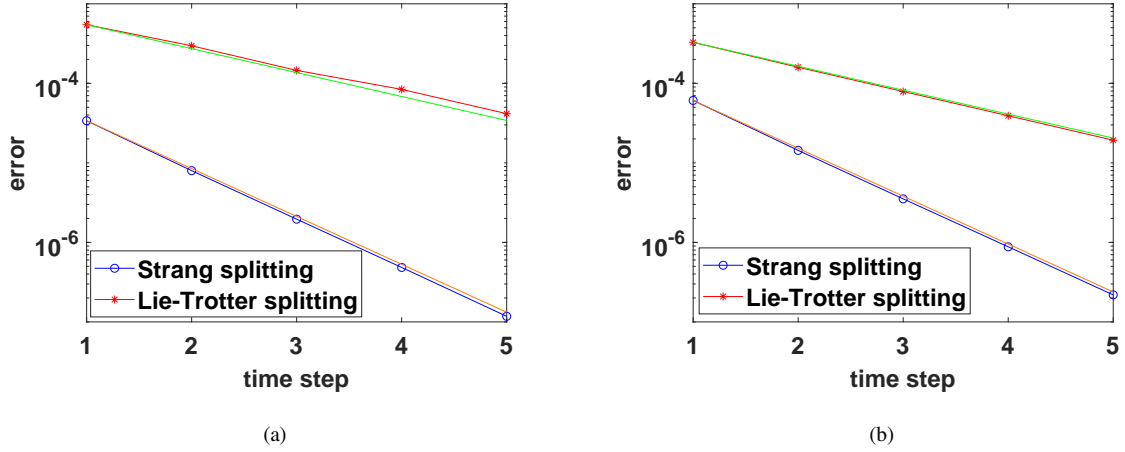


Figure 2: Convergence rates of numerical solutions with respect to time step. (a): Error of position; (b): Error of velocity. The solid colored lines refer to the corresponding theoretical value.

We check the convergence order of splitting methods in Figure 2 for Landau damping with $k = 0.5$. We start from choosing $\Delta t_0 = 0.5$ and once again conduct four runs by decreasing the time step with each run. That is, the time steps can be chosen as $\Delta t_i = 2^{-(i+1)}$, $i = 1, 2, 3, 4$. We use e_i^x to denote the error of position with time step Δt_i . For a fixed final time T , the error order can be calculated by $\log(e_j^x/e_{j+1}^x)/\log(\Delta t_j/\Delta t_{j+1})$, $j = 0, 1, 2, 3, 4$. Similarly, we can calculate the error order of velocity. As it shown in the figure, the numerical results by Strang splitting perform much better than the ones by Lie-Trotter splitting due to the higher-order accuracy of Strang splitting method. However, the damping rates by both approaches can match the analytical ones.

Two-stream instability. Two-stream is a common instability in plasma physics which occurs when an energetic particle stream injects into a plasma, or a current is set along the plasma. The phenomena can be investigated when there exists (time-depending) difference of drift velocity between two plasma components. In our simulation, for the

initial value we set a perturbation as a vortex creation at the center of concerned domain. That is, the initial datum can be set as

$$f_0(x, v) = \frac{1}{\sqrt{2\pi}} v^2 \exp\left(-\frac{v^2}{2}\right) (1 + \alpha \cos(kx)),$$

where perturbation parameter $\alpha = 0.01$ and wave number $k = 0.5$. The computation domain is $[0, 2\pi/k] \times [-5, 5]$. We take Δt and N_x as shown in the above experiments.

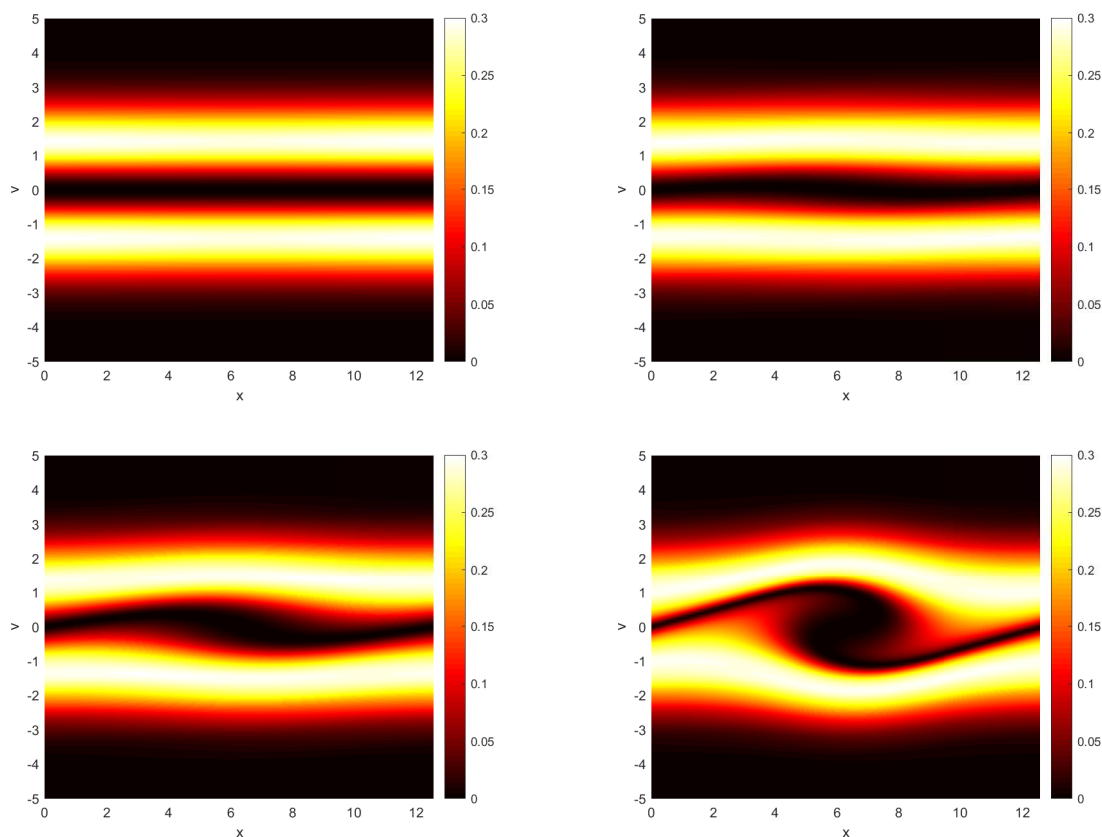


Figure 3: Evolution of the distribution f for time $t = 0, 10, 15, 20$.

In Figure 3, we plot the distribution function f for time $t = 0, 10, 15, 20$. It is observed that the instability appears quickly, and the obvious vortex structure can be captured clearly. This coincides with the instability phenomenon shown in literature [4, 16].

In Figure 4, we plot the total energy and momentum. We can observe that our method can preserve the energy and momentum well over long-time even when the instability occurs.

Bump-on-tail instability. Bump-on-tail instability is a fundamental example of wave-particle interaction, the instability can be investigated when the wave and particles interact. In this test, for studying the Bump-on-tail instability we take the following initial conditions [54]

$$f_0(x, v) = (1 + \alpha \cos(kx))d_0(v),$$

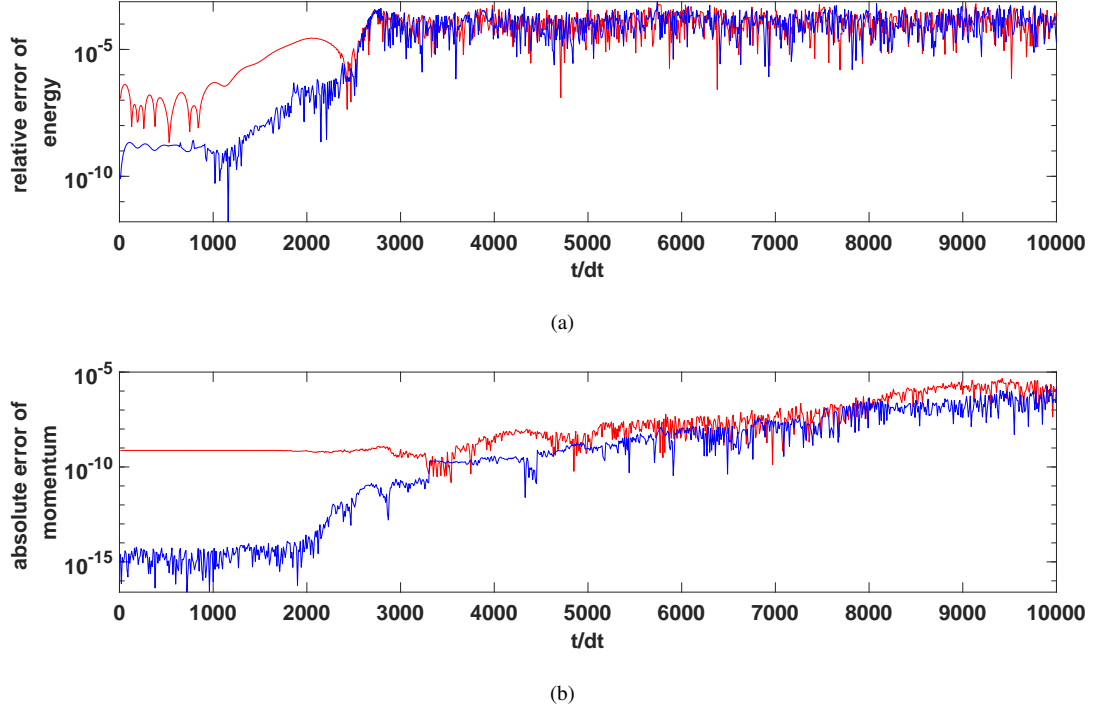


Figure 4: Time evolutions of conservative quantities for Two-stream instability. (a): Error of energy; (b): Error of momentum. The red line shows the error by the Lie-Trotter splitting while the blue line refers to the ones by the Strang splitting.

where perturbation parameter $\alpha = 0.04$ and wave number $k = 0.3$. In the above initial value, d_0 denotes a bump on the tail of distribution function formed by energetic particles, which has the following expression

$$d_0 = \frac{1}{\sqrt{2\pi}} \left(0.9 \exp\left(-\frac{v^2}{2}\right) + 0.2 \exp(-2(v - 4.5)^2) \right).$$

In this experiment, computation domain $[0, 6\pi/k] \times [-8, 8]$ is considered. We choose $\Delta t = 0.01$ and $N_x = 256$ to simulate this problem. In Figure 5, we plot the distribution function f for time $t = 0, 10, 15, 20$. It is observed that our numerical discretization can describe the evolution of instability and the occurrence phenomena. Clearly, it is investigated that there appear three vortices which extending arms embrace the neighbouring vortices.

It should be noticed that implementing our numerical method involves computations in a large amount of cycles which can be treated in parallel. As follows, we show the efficiency of our numerical computation together with the parallel approach. Based on MPI, we take two natural parallel strategies for the collective communications in the cycle. For particle deposition part, the computational domain is subdivided into regions while for pushing particle part, the particles are divided into groups. For the first strategy, we can also improve it by using, for instance, the adaptive scheme presented in [43]. In Figure 6, we present the speed-up comparison for our numerical computation and the ideal ones. By comparison, it can be seen that our speed-up result is quite good due to the so-called cache effects.

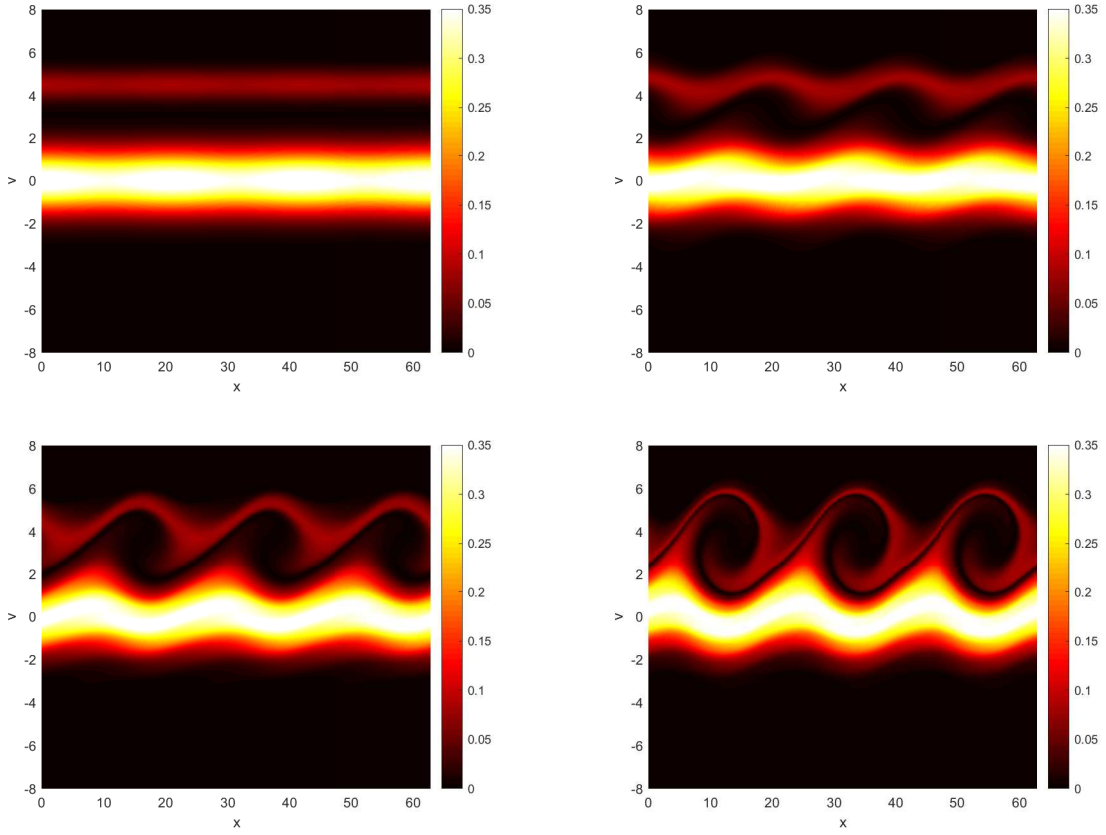


Figure 5: Time evolution of the distribution f for time $t = 0, 10, 15, 20$.

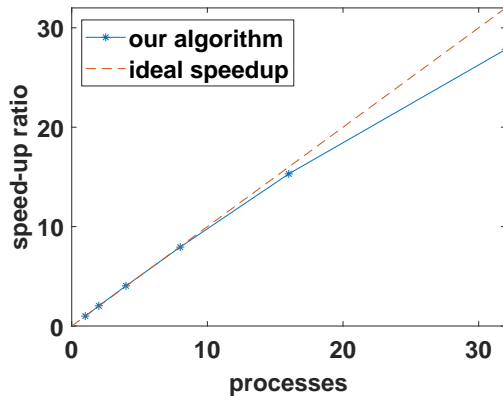


Figure 6: Speed-up of numerical computing for simulating Bump-on-tail instability on LSSC-IV. The computation is done by taking 10^5 particles in phase space.

6.2. Test problems in 2+2-dimensional phase space

In this experiment, we consider the Vlasov–Poisson system in 2+2-dimension which means 2D in space and also 2D in velocity one. We assign $N_x = N_y = 256$ for the initial particle grid and 250 particles per cell. This means that we take over 10^7 particles for the simulation.

Diocotron instability. The diocotron instability is a plasma instability which occurs when two sheets of charges slipping past each other. This stability is usually described by the guiding center model [37, 22, 1] and has been extensively simulated [15, 22, 26, 1, 9]. Here, we consider the model of two dimensional Vlasov–Poisson system together with an external magnetic field. This system can be taken to model the instability which is usually encountered in magnetic fusion devices such as tokamaks. In this example, we also consider the effect of magnetic field to the instability. Thus, we consider the case with strong magnetic field. As the instability usually is explained as the analog of the Kelvin-Helmholtz instability in fluid mechanics, it can be observed directly in the nature [50]. In this situation, the energy of system is dissipated as the two surface waves propagate in two opposite directions with one flowing over the other. By investigation, there appears the vortex structure in the surface of distribution function when the instability happens [22, 26, 1].

The Vlasov equation in this simulation is with an external magnetic field \mathbf{B}_{ext} which reads

$$\varepsilon \frac{\partial f}{\partial t} + \mathbf{v} \cdot \frac{\partial f}{\partial \mathbf{x}} + (\mathbf{E}(t, \mathbf{x}) + \frac{1}{\varepsilon} \mathbf{v} \times \mathbf{B}_{\text{ext}}(t, \mathbf{x})) \cdot \frac{\partial f}{\partial \mathbf{v}} = 0.$$

Here, ε is the strength of magnetic field. As the parameter ε is usually small, the existence of term ε in front of the time derivative of f requires the numerical simulations to have long-time stability. There have been many numerical methods for studying this instability. Among them, the asymptotic preserving schemes are introduced in [26], and the uniformly accurate methods are introduced in [9].

We take the initial distribution function as

$$f_0(\mathbf{x}, \mathbf{v}) = \frac{d_0(\mathbf{x})}{2\pi} \exp\left(-\frac{\|\mathbf{v}\|^2}{2}\right), \quad \mathbf{x} = (x, y) \in \mathbb{R}^2,$$

where the initial density is

$$d_0(\mathbf{x}) = \begin{cases} (1 + \alpha \cos(l\theta)) \exp(-4(\|\mathbf{x}\| - 6.5)^2) & \text{if } r^- \leq \|\mathbf{x}\| \leq r^+, \\ 0 & \text{otherwise,} \end{cases}$$

with $\theta = \text{atan}(y/x)$ and l the number of vortices. In our simulation, we take $r^- = 5$, $r^+ = 8$, $\alpha = 0.2$ and $\mathbf{B}_{\text{ext}} = (0, 0, 1)$.

In Figure 7, we consider the case where ε is taken as $\varepsilon = 1$. We use $\Delta t = 0.1$ and $l = 7$ for this case. It can be observed that the plasma is not well confined. This can be explained that the enforced magnetic field is not strong enough. This phenomena is also performed in [22]. Though the vortices will not occur, it still can be observed that for the case of $l = 7$ there are seven clear clusters changing along the time.

Then, we take a small value of $\varepsilon = 0.1$ in Figure 8 and $\varepsilon = 0.01$ in Figure 9. In our computation, we use $\Delta t = 0.1$ and $\Delta t = 0.01$ respectively.

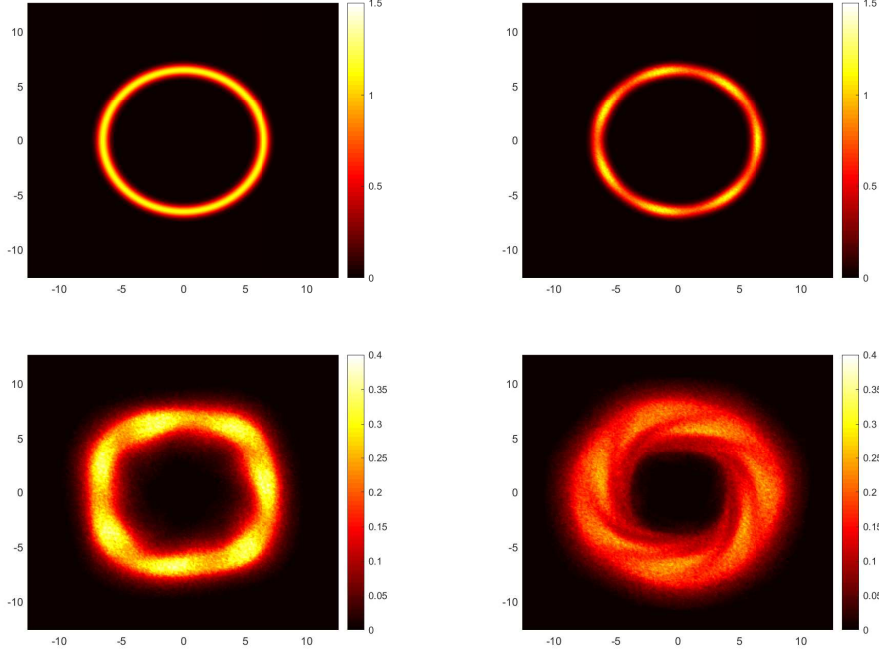


Figure 7: Time evolution of the density ρ for time $t = 0, 0.1, 15, 30$ and $l = 7$ with strength of magnetic field $\varepsilon = 1$.

We plot the development of the diocotron instability at different time with $l = 5$ in Figure 8. It is observed that the five vortex structures are well captured by our method. If we change the direction of magnetic field, it can be observed in this figure that the vortex structure will move on the reversed direction.

From Figure 9, it can be observed that the vortex structures become smaller when the magnetic field is stronger. Also, the image becomes not clear. To improve this more particles in practical computation are needed and finer resolution should be applied. The computational cost can still be distributed efficiently due to the parallel approach used in this paper.

7. Conclusion

In this work, we have developed the symplectic Particle-in-Cell methods for solving the Vlasov–Poisson system according to its Poisson bracket. We use the appropriate finite element spaces so that the semi-discrete system is equipped with a discrete Poisson structure. With regard to temporal discretization, we apply the splitting technique. As each subsystem can be solved exactly, the resulting discretization can preserve the Poisson structure of the concerning system. In order to implement efficiently our algorithm, parallel computing technique has been designed, and applied to various problems. The parallel efficiency of practical computation has been verified via the numerical results of this experiments. We also show the convergence rates of splitting methods of first and second order which are taken as a benchmark test. The numerical results perform that they all match the theoretical order very well. To verify

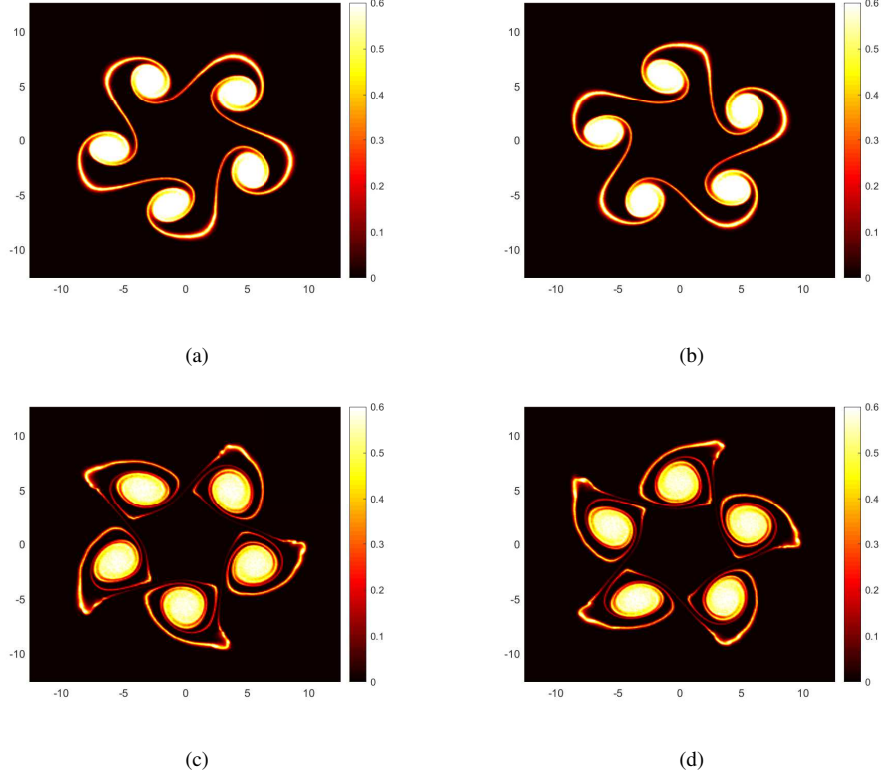


Figure 8: Time evolution of the density ρ along the time. (a): $\mathbf{B}_{\text{ext}} = (0, 0, 1)$, $t = 30$; (b): $\mathbf{B}_{\text{ext}} = (0, 0, -1)$, $t = 30$; (c): $\mathbf{B}_{\text{ext}} = (0, 0, 1)$, $t = 50$; (d) $\mathbf{B}_{\text{ext}} = (0, 0, -1)$, $t = 50$. Here $l = 5$ and the strength of magnetic field is $\varepsilon = 0.1$.

the advantage of Poisson bracket preserving methods constructed in this paper, we study the preservation of energy both theoretically and numerically. This guarantees the numerical simulation over long-time. We also present a 2+2-dimensional example, in this example the external magnetic field can be strong. The error and stability analysis of the derived numerical methods will be reported in the future publications.

8. Acknowledgments

This research was supported by the National Natural Science Foundation of China (11771436,11505185), the National Key R&D Program of China (2017YFE0301704).

Appendix A. Jacobi identity of the continuous bracket

In this section we prove the Jacobi identity of the bracket (7) when $\nabla \cdot \mathbf{B}_0 = 0$. To simplify the notation, we use $[\cdot, \cdot]$ to replace the continuous bracket $\{\{\cdot, \cdot\}\}$ in this section.

Following the idea in [44], we rewrite the continuous bracket (7) as two parts,

$$[\mathcal{F}, \mathcal{G}] = [\mathcal{F}, \mathcal{G}]_{xv} + [\mathcal{F}, \mathcal{G}]_B.$$

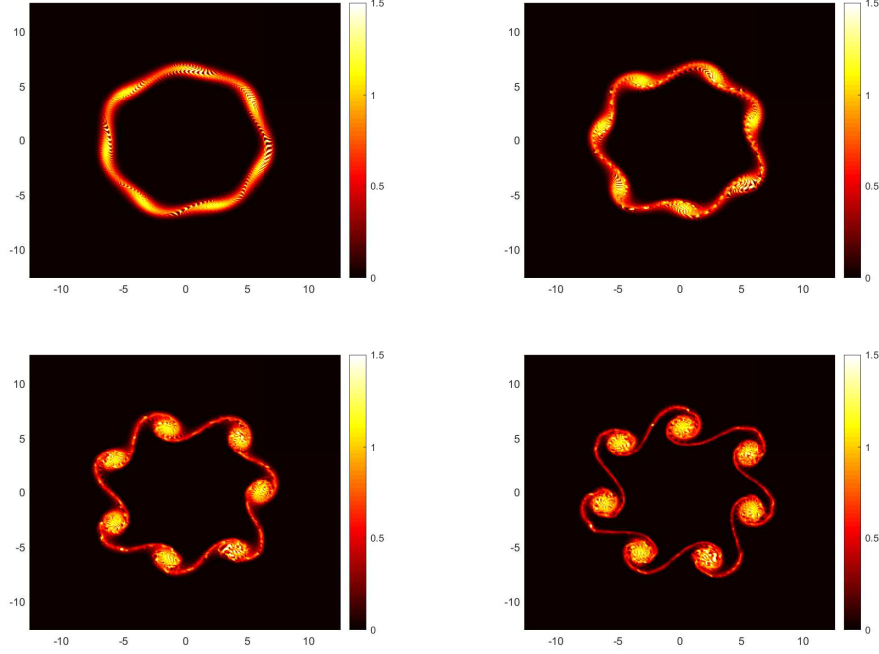


Figure 9: Time evolution of the density ρ for time $t = 5, 10, 15, 20$ and $l = 7$ with strength of magnetic field $\varepsilon = 0.01$.

Each part in the form can be written as

$$[\mathcal{F}, \mathcal{G}]_{xv}(f) = \int_{\Omega_x \times \Omega_v} f \left\{ \frac{\delta \mathcal{F}}{\delta f}, \frac{\delta \mathcal{G}}{\delta f} \right\}_{xv} dx dv$$

$$[\mathcal{F}, \mathcal{G}]_B(f) = \int_{\Omega_x \times \Omega_v} f \mathbf{B}_0 \cdot \left(\frac{\partial}{\partial \mathbf{v}} \frac{\delta \mathcal{F}}{\delta f} \times \frac{\partial}{\partial \mathbf{v}} \frac{\delta \mathcal{G}}{\delta f} \right) dx dv.$$

Then the Jacobi identity reads

$$[\mathcal{F}, \mathcal{H}] + cyc = \underbrace{[[\mathcal{F}, \mathcal{G}]_{xv}, \mathcal{H}]_{xv}}_1 + \underbrace{[[\mathcal{F}, \mathcal{G}]_{xv}, \mathcal{H}]_B}_2$$

$$+ \underbrace{[[\mathcal{F}, \mathcal{G}]_B, \mathcal{H}]_{xv}}_3 + \underbrace{[[\mathcal{F}, \mathcal{G}]_B, \mathcal{H}]_B}_4$$

$$+ cyc,$$

where the symbol *cyc* means cyclic permutation.

Term 1 vanishes because of the Jacobi identity of $\{ \cdot, \cdot \}_{xv}$. It is also the bracket of VP equation under $\mathbf{B}_0 = \mathbf{0}$, see [40, 8].

Next, we simplify the notations. Let $\delta \mathcal{F} = \frac{\delta \mathcal{F}}{\delta f}$, $\delta \mathcal{G} = \frac{\delta \mathcal{G}}{\delta f}$, $\delta \mathcal{H} = \frac{\delta \mathcal{H}}{\delta f}$ and $\alpha = \frac{\partial}{\partial \mathbf{v}} \delta \mathcal{F}$, $\beta = \frac{\partial}{\partial \mathbf{v}} \delta \mathcal{G}$, $\gamma = \frac{\partial}{\partial \mathbf{v}} \delta \mathcal{H}$. And we use \mathbf{B}_i or α_i to denote the i -th component of \mathbf{B}_0 or α . Then term 2+3 reads

$$\int_{\Omega_x \times \Omega_v} f \mathbf{B}_0 \cdot \left(\frac{\partial}{\partial \mathbf{v}} \{ \delta \mathcal{F}, \delta \mathcal{G} \}_{xv} \times \gamma \right) + f \{ \mathbf{B}_0 \cdot (\alpha \times \beta), \delta \mathcal{H} \}_{xv} dx dv.$$

Notice that $(u \times v)_i = \sum_{jk} \epsilon_{ijk} u_j v_k$ for two vectors u, v ,

$$\begin{aligned} & \mathbf{B}_0 \cdot \left(\frac{\partial}{\partial \mathbf{v}} \{ \delta \mathcal{F}, \delta \mathcal{G} \}_{\mathbf{xv}} \times \gamma \right) + \{ \mathbf{B}_0 \cdot (\alpha \times \beta), \delta \mathcal{H} \}_{\mathbf{xv}} \\ &= \sum_{ijk} \epsilon_{ijk} \mathbf{B}_i (\{ \alpha_j, \delta \mathcal{G} \}_{\mathbf{xv}} + \{ \delta \mathcal{F}, \beta_j \}_{\mathbf{xv}}) \gamma_k + \sum_{ijk} \epsilon_{ijk} \{ \mathbf{B}_i \alpha_j \beta_k, \delta \mathcal{H} \}_{\mathbf{xv}}, \end{aligned}$$

where ϵ_{ijk} is the Levi-Civita symbol. As \mathbf{B}_0 is independent of \mathbf{v} , the third term on the right side of the above equality reads

$$\begin{aligned} & \{ \mathbf{B}_i \alpha_j \beta_k, \delta \mathcal{H} \}_{\mathbf{xv}} \\ &= \sum_l \left(\frac{\partial}{\partial \mathbf{x}_l} (\mathbf{B}_i \alpha_j \beta_k) \gamma_l - \mathbf{B}_i \frac{\partial}{\partial \mathbf{v}_l} (\alpha_j \beta_k) \frac{\partial}{\partial \mathbf{x}_l} \delta \mathcal{H} \right) \\ &= \mathbf{B}_i \{ \alpha_j \beta_k, \delta \mathcal{H} \}_{\mathbf{xv}} + \sum_l \frac{\partial}{\partial \mathbf{x}_l} \mathbf{B}_i (\alpha_j \beta_k \gamma_l). \end{aligned}$$

By Leibniz' rule of $\{ \cdot, \cdot \}_{\mathbf{xv}}$, it is known that

$$\begin{aligned} & \{ \alpha_j, \delta \mathcal{G} \}_{\mathbf{xv}} \gamma_k + \{ \delta \mathcal{F}, \beta_j \}_{\mathbf{xv}} \gamma_k + \{ \alpha_j \beta_k, \delta \mathcal{H} \}_{\mathbf{xv}} \\ &= \{ \alpha_j, \delta \mathcal{G} \}_{\mathbf{xv}} \gamma_k + \{ \delta \mathcal{F}, \beta_j \}_{\mathbf{xv}} \gamma_k + \{ \beta_k, \delta \mathcal{H} \}_{\mathbf{xv}} \alpha_j + \{ \alpha_j, \delta \mathcal{H} \}_{\mathbf{xv}} \beta_k \\ &= \underbrace{(\{ \alpha_j, \delta \mathcal{G} \}_{\mathbf{xv}} \gamma_k + \{ \beta_k, \delta \mathcal{H} \}_{\mathbf{xv}} \alpha_j)}_{\mathcal{A}} + \underbrace{(\{ \delta \mathcal{F}, \beta_j \}_{\mathbf{xv}} \gamma_k + \{ \alpha_j, \delta \mathcal{H} \}_{\mathbf{xv}} \beta_k)}_{\mathcal{B}}. \end{aligned}$$

The terms $\sum_{ijk} \epsilon_{ijk} \mathbf{B}_i \mathcal{A}$ and $\sum_{ijk} \epsilon_{ijk} \mathbf{B}_i \mathcal{B}$ cancel out by permuting \mathcal{F} , \mathcal{G} and \mathcal{H} . Notice that $\sum_{ijk} \sum_l \epsilon_{ijk} \frac{\partial}{\partial \mathbf{x}_l} \mathbf{B}_i (\alpha_j \beta_k \gamma_l) = \sum_l \frac{\partial}{\partial \mathbf{x}_l} \mathbf{B}_0 \cdot (\alpha \times \beta) \gamma_l$ and $(\alpha \times \beta)_i \gamma_j + c_{yc} = \delta_{ij} (\alpha \times \beta) \cdot \gamma$, the summation of terms 2 and 3 leads to $\int_{\Omega_x \times \Omega_v} f(\nabla \cdot \mathbf{B}_0) ((\alpha \times \beta) \cdot \gamma) d\mathbf{x} d\mathbf{v}$ which vanishes when $\nabla \cdot \mathbf{B}_0 = 0$.

According to the above notations, term 4 reads

$$\int_{\Omega_x \times \Omega_v} f \mathbf{B}_0 \cdot \left(\frac{\partial}{\partial \mathbf{v}} (\mathbf{B}_0 \cdot (\alpha \times \beta)) \times \gamma \right) d\mathbf{x} d\mathbf{v}$$

By calculation, it is

$$\begin{aligned} & \mathbf{B}_0 \cdot \left(\frac{\partial}{\partial \mathbf{v}} (\mathbf{B}_0 \cdot (\alpha \times \beta)) \times \gamma \right) \\ &= \sum_{ijk} \sum_{lmn} \epsilon_{ijk} \epsilon_{lmn} \mathbf{B}_i \mathbf{B}_l \left(\frac{\partial}{\partial \mathbf{v}_j} \alpha_m \beta_n \right) \gamma_k \\ &= \sum_{ijk} \sum_{lmn} \epsilon_{ijk} \epsilon_{lmn} \mathbf{B}_i \mathbf{B}_l (\alpha_m \beta_n \gamma_k + \alpha_m \beta_n \gamma_k), \end{aligned}$$

where α_{mj} means $\frac{\partial}{\partial \mathbf{v}_j} \alpha_m$.

By shifting the indices $i \rightarrow l, j \rightarrow m, k \rightarrow n, l \rightarrow i, m \rightarrow k, n \rightarrow j$ and $\alpha \beta \gamma \rightarrow \gamma \alpha \beta$, $\epsilon_{ijk} \epsilon_{lmn} \mathbf{B}_i \mathbf{B}_l \alpha_m \beta_n \gamma_k \rightarrow \epsilon_{lmn} \epsilon_{ikj} \mathbf{B}_l \mathbf{B}_i \gamma_k \alpha_j \beta_n$.

Then term 4 vanishes accordingly due to the anti-symmetry of the Levi-Civita symbol.

By the above calculation, we conclude that the continuous bracket (7) is Poisson if $\nabla \cdot \mathbf{B}_0 = 0$.

Appendix B. Derivation of the discrete Poisson bracket

As follows, we prove that the particle system (12) with the approximate electric field (17) is still a Hamiltonian system with the defined discrete Poisson bracket. Under the approximation (11), we denote a functional of f_h as

$$\mathcal{F}[f_h] = F(\omega, \mathbf{X}, \mathbf{V}).$$

Denote

$$f_s(\mathbf{x}, \mathbf{v}, t) = \omega_s \delta(\mathbf{x} - \mathbf{X}_s) \delta(\mathbf{v} - \mathbf{V}_s), s = 1, 2, \dots, N_p.$$

The discrete variables can be reexpressed by $\omega_s = \int f_s d\mathbf{x}d\mathbf{v}$, $\mathbf{X}_s = \frac{1}{\omega_s} \int \mathbf{x} f_s d\mathbf{x}d\mathbf{v}$ and $\mathbf{V}_s = \frac{1}{\omega_s} \int \mathbf{v} f_s d\mathbf{x}d\mathbf{v}$. Taking their derivatives w.r.t f_s providing

$$\frac{\delta \omega_s}{\delta f_s} = 1, \quad \frac{\delta \mathbf{X}_s}{\delta f_s} = \frac{\mathbf{x} - \mathbf{X}_s}{\omega_s}, \quad \frac{\delta \mathbf{V}_s}{\delta f_s} = \frac{\mathbf{v} - \mathbf{V}_s}{\omega_s}.$$

Notice that $\frac{\delta \mathcal{F}}{\delta f_h} = \sum_s \frac{\delta \mathcal{F}}{\delta f_s}$. Using the chain rule of variation to calculate $\frac{\delta \mathcal{F}}{\delta f_s}$ gives

$$\begin{aligned} \frac{\delta \mathcal{F}}{\delta f_s} &= \frac{\delta \omega_s}{\delta f_s} \frac{\partial F}{\partial \omega_s} + \frac{\delta \mathbf{X}_s}{\delta f_s} \frac{\partial F}{\partial \mathbf{X}_s} + \frac{\delta \mathbf{V}_s}{\delta f_s} \frac{\partial F}{\partial \mathbf{V}_s} \\ &= \frac{\partial F}{\partial \omega_s} + \frac{\mathbf{x} - \mathbf{X}_s}{\omega_s} \frac{\partial F}{\partial \mathbf{X}_s} + \frac{\mathbf{v} - \mathbf{V}_s}{\omega_s} \frac{\partial F}{\partial \mathbf{V}_s}. \end{aligned}$$

It leads to

$$\begin{aligned} \left\{ \frac{\delta \mathcal{F}}{\delta f_s}, \frac{\delta \mathcal{G}}{\delta f_s} \right\}_{\mathbf{xv}} &= \left\{ \frac{\partial F}{\partial \omega_s} + \frac{\mathbf{x} - \mathbf{X}_s}{\omega_s} \frac{\partial F}{\partial \mathbf{X}_s} + \frac{\mathbf{v} - \mathbf{V}_s}{\omega_s} \frac{\partial F}{\partial \mathbf{V}_s}, \frac{\partial G}{\partial \omega_s} + \frac{\mathbf{x} - \mathbf{X}_s}{\omega_s} \frac{\partial G}{\partial \mathbf{X}_s} + \frac{\mathbf{v} - \mathbf{V}_s}{\omega_s} \frac{\partial G}{\partial \mathbf{V}_s} \right\}_{\mathbf{xv}} \\ &= \frac{1}{\omega_s^2} \left(\frac{\partial F}{\partial \mathbf{X}_s} \cdot \frac{\partial G}{\partial \mathbf{V}_s} - \frac{\partial F}{\partial \mathbf{V}_s} \cdot \frac{\partial G}{\partial \mathbf{X}_s} \right), \end{aligned}$$

Then

$$\int_{\Omega_x \times \Omega_v} f_h \left\{ \frac{\delta \mathcal{F}}{\delta f_h}, \frac{\delta \mathcal{G}}{\delta f_h} \right\}_{\mathbf{xv}} d\mathbf{x}d\mathbf{v} = \sum_{s=1}^{N_p} \frac{1}{\omega_s} \left(\frac{\partial F}{\partial \mathbf{X}_s} \cdot \frac{\partial G}{\partial \mathbf{V}_s} - \frac{\partial F}{\partial \mathbf{V}_s} \cdot \frac{\partial G}{\partial \mathbf{X}_s} \right).$$

And

$$\begin{aligned} \int_{\Omega_x \times \Omega_v} f_h \mathbf{B}_0(\mathbf{x}) \cdot \left(\frac{\partial}{\partial \mathbf{v}} \frac{\delta \mathcal{F}}{\delta f_h} \times \frac{\partial}{\partial \mathbf{v}} \frac{\delta \mathcal{G}}{\delta f_h} \right) d\mathbf{x}d\mathbf{v} &= \int_{\Omega_x \times \Omega_v} f_h \mathbf{B}_0(\mathbf{x}) \cdot \left(\frac{1}{\omega_s^2} \frac{\partial F}{\partial \mathbf{V}_s} \times \frac{\partial G}{\partial \mathbf{V}_s} \right) d\mathbf{x}d\mathbf{v} \\ &= \sum_{s=1}^{N_p} \frac{1}{\omega_s} \mathbf{B}_0(\mathbf{X}_s) \cdot \left(\frac{\partial F}{\partial \mathbf{V}_s} \times \frac{\partial G}{\partial \mathbf{V}_s} \right). \end{aligned}$$

Therefore, we can define the following discrete bracket operator as

$$\{F, G\}(\mathbf{X}, \mathbf{V}) = \sum_{s=1}^{N_p} \frac{1}{\omega_s} \left(\frac{\partial F}{\partial \mathbf{X}_s} \cdot \frac{\partial G}{\partial \mathbf{V}_s} - \frac{\partial F}{\partial \mathbf{V}_s} \cdot \frac{\partial G}{\partial \mathbf{X}_s} \right) + \sum_{s=1}^{N_p} \frac{1}{\omega_s} \mathbf{B}_0(\mathbf{X}_s) \cdot \left(\frac{\partial F}{\partial \mathbf{V}_s} \times \frac{\partial G}{\partial \mathbf{V}_s} \right).$$

Appendix C. Jacobi identity of the discrete bracket

As follows, we prove that the discrete bracket (19) is a Poisson bracket under $\nabla \cdot \mathbf{B}_0(\mathbf{x}) = 0$.

At the end of section 4, we connect the discrete Poisson bracket (19) which derivation has been shown in Appendix B to a matrix \mathbb{K} which is called the Poisson matrix. Thus, the discrete bracket is Poisson if and only if for the component of matrix \mathbb{K} the following identity holds for all i, j, k

$$\sum_{l=1}^{6N_p} \left(\frac{\partial \mathbb{K}_{ij}}{\partial \mathbf{Z}^l} \mathbb{K}_{lk} + \frac{\partial \mathbb{K}_{jk}}{\partial \mathbf{Z}^l} \mathbb{K}_{li} + \frac{\partial \mathbb{K}_{ki}}{\partial \mathbf{Z}^l} \mathbb{K}_{lj} \right) = 0,$$

where \mathbf{Z}^l is the l -th component of $\hat{\mathbf{Z}}$, see [48, 29].

It can be known that

$$\begin{aligned} & \sum_{l=1}^{6N_p} \left(\frac{\partial \mathbb{K}_{ij}}{\partial \mathbf{Z}^l} \mathbb{K}_{lk} + \frac{\partial \mathbb{K}_{jk}}{\partial \mathbf{Z}^l} \mathbb{K}_{li} + \frac{\partial \mathbb{K}_{ki}}{\partial \mathbf{Z}^l} \mathbb{K}_{lj} \right) \\ &= \sum_{l=1}^{3N_p} \left(\frac{\partial \mathbb{N}^{-1} \hat{\mathbb{B}}(\mathbf{X})_{ij}}{\partial \mathbf{X}^l} \mathbb{N}_{lk}^{-1} + \frac{\partial \mathbb{N}^{-1} \hat{\mathbb{B}}(\mathbf{X})_{jk}}{\partial \mathbf{X}^l} \mathbb{N}_{li}^{-1} + \frac{\partial \mathbb{N}^{-1} \hat{\mathbb{B}}(\mathbf{X})_{ki}}{\partial \mathbf{X}^l} \mathbb{N}_{lj}^{-1} \right). \end{aligned}$$

Due to that \mathbb{N} is a diagonal constant matrix, the right term of the above equality leads to

$$\frac{\partial \mathbb{N}^{-1} \hat{\mathbb{B}}(\mathbf{X})_{ij}}{\partial \mathbf{X}^k} \mathbb{N}_{kk}^{-1} + \frac{\partial \mathbb{N}^{-1} \hat{\mathbb{B}}(\mathbf{X})_{jk}}{\partial \mathbf{X}^i} \mathbb{N}_{ii}^{-1} + \frac{\partial \mathbb{N}^{-1} \hat{\mathbb{B}}(\mathbf{X})_{ki}}{\partial \mathbf{X}^j} \mathbb{N}_{jj}^{-1}.$$

If \mathbf{X}^i and \mathbf{X}^j are not the components for the same particle position \mathbf{X}_s , then $\frac{\partial \mathbb{N}^{-1} \hat{\mathbb{B}}(\mathbf{X})_{ij}}{\partial \mathbf{X}^k} \mathbb{N}_{kk}^{-1} + \frac{\partial \mathbb{N}^{-1} \hat{\mathbb{B}}(\mathbf{X})_{jk}}{\partial \mathbf{X}^i} \mathbb{N}_{ii}^{-1} + \frac{\partial \mathbb{N}^{-1} \hat{\mathbb{B}}(\mathbf{X})_{ki}}{\partial \mathbf{X}^j} \mathbb{N}_{jj}^{-1} = 0$ due to that the value of all partial derivatives of functions is zero. Therefore, we only need to consider the case in which $\mathbf{X}^i, \mathbf{X}^j, \mathbf{X}^k$ are the components for the same particle position \mathbf{X}_s . This reads

$$\frac{1}{\omega_s^2} \left(\frac{\partial \hat{\mathbb{B}}_{ij}}{\partial \mathbf{X}^k} + \frac{\partial \hat{\mathbb{B}}_{jk}}{\partial \mathbf{X}^i} + \frac{\partial \hat{\mathbb{B}}_{ki}}{\partial \mathbf{X}^j} \right) = 0.$$

In the above equality, if the two of three indexes are equal the terms related cancel out because of the skew-symmetry of matrix $\hat{\mathbb{B}}$. With the Levi-Civita symbol ϵ_{ijk} , it is known that $\hat{\mathbb{B}}_{ij}$ has the expression $\hat{\mathbb{B}}_{ij} = \epsilon_{ijk} \mathbf{B}_0(\mathbf{X}_s)_k$ when the three indices are different. Then $\frac{\partial \hat{\mathbb{B}}_{ij}}{\partial \mathbf{X}^k} + \frac{\partial \hat{\mathbb{B}}_{jk}}{\partial \mathbf{X}^i} + \frac{\partial \hat{\mathbb{B}}_{ki}}{\partial \mathbf{X}^j} = 0$ if and only if $\nabla_{\mathbf{X}_s} \cdot \mathbf{B}_0(\mathbf{X}_s) = 0$. This implies the bracket defined by \mathbb{K} is Poisson if $\nabla \cdot \mathbf{B}_0(\mathbf{x}) = 0$.

References

- [1] Jakob Ameres. *Stochastic and spectral particle methods for plasma physics*. PhD thesis, Technische Universität München, 2018.
- [2] Aurore Back and Eric Sonnendrücker. Finite Element Hodge for spline discrete differential forms. Application to the Vlasov–Poisson system. *Applied Numerical Mathematics*, 79:124–136, 2014.
- [3] Weizhu Bao, Xuanchun Dong, and Xiaofei Zhao. Uniformly accurate multiscale time integrators for highly oscillatory second order differential equations. *Journal of Mathematical Study*, 47(2):111–150, 2014.
- [4] Nicolas Besse and Eric Sonnendrücker. Semi-Lagrangian schemes for the Vlasov equation on an unstructured mesh of phase space. *Journal of Computational Physics*, 191(2):341–376, 2003.
- [5] C. K. Birdsall and A. B. Langdon. *Plasma Physics Via Computer Simulation*. CRC Press, 1991.
- [6] Susanne C. Brenner and L. Ridgway Scott. *The Mathematical Theory of Finite Element Methods*. Texts in Applied Mathematics. Springer, New York, 2008.

- [7] J. W. Burby. Finite-dimensional collisionless kinetic theory. *Physics of Plasmas*, 24(3):032101, 2017.
- [8] Fernando Casas, Nicolas Crouseilles, Erwan Faou, and Michel Mehrenberger. High-order Hamiltonian splitting for Vlasov–Poisson equations. *Numerische Mathematik*, 135(3):769–801, 2017.
- [9] Philippe Chartier, Nicolas Crouseilles, Mohammed Lemou, Florian Méhats, and Xiaofei Zhao. Uniformly accurate methods for three dimensional Vlasov equations under strong magnetic field with varying direction. *SIAM Journal on Scientific Computing*, 42(2):B520–B547, 2020.
- [10] G. Chen, L. Chacón, and D.C. Barnes. An energy- and charge-conserving, implicit, electrostatic particle-in-cell algorithm. *Journal of Computational Physics*, 230(18):7018–7036, 2011.
- [11] Yingda Cheng, Andrew J. Christlieb, and Xinghui Zhong. Energy-conserving discontinuous Galerkin methods for the Vlasov–Ampère system. *Journal of Computational Physics*, 256:630–655, 2014.
- [12] G.-H. Cottet and P.-A. Raviart. Particle methods for the one-dimensional Vlasov–Poisson equations. *SIAM Journal on Numerical Analysis*, 21(1):52–76, 1984.
- [13] Georges-Henri Cottet and Petros D. Koumoutsakos. *Vortex Methods: Theory and Practice*. Cambridge University Press, 2000.
- [14] Nicolas Crouseilles, Lukas Einkemmer, and Erwan Faou. Hamiltonian splitting for the Vlasov–Maxwell equations. *Journal of Computational Physics*, 283:224–240, 2015.
- [15] Nicolas Crouseilles, Pierre Glanc, Sever Adrian Hirstoaga, Eric Madaule, Michel Mehrenberger, and Jérôme Pétri. A new fully two-dimensional conservative semi-Lagrangian method: applications on polar grids, from diocotron instability to ITG turbulence. *The European Physical Journal D*, 68(252), 2014.
- [16] Nicolas Crouseilles, Guillaume Latu, and Eric Sonnendrücker. A parallel Vlasov solver based on local cubic spline interpolation on patches. *Journal of Computational Physics*, 228(5):1429–1446, 2009.
- [17] Nicolas Crouseilles and Thomas Respaud. A charge preserving scheme for the numerical resolution of the Vlasov–Ampère equations. *Communications in Computational Physics*, 10(4):1001–1026, 2011.
- [18] E. G. Evstatiev and B. A. Shadwick. Variational formulation of particle algorithms for kinetic plasma simulations. *Journal of Computational Physics*, 245:376–398, 2013.
- [19] Kang Feng. Proceedings of the 1984 Beijing Symposium of Differential Geometry and Differential Equations–Computation of Partial Differential Equation. *Science Press, Beijing*, page 42–58, 1985.
- [20] Kang Feng. *Collected Works of Feng Kang*. National Defence Industry Press, Beijing, China, 1995.
- [21] Kang Feng and Mengzhao Qin. *Symplectic Geometric Algorithms for Hamiltonian Systems*. Springer, Berlin, Heidelberg, 2010.
- [22] Francis Filbet and Luis Miguel Rodrigues. Asymptotically stable Particle-in-Cell methods for the Vlasov–Poisson system with a strong external magnetic field. *SIAM Journal on Numerical Analysis*, 54(2):1120–1146, 2016.
- [23] Francis Filbet and Eric Sonnendrücker. Comparison of Eulerian Vlasov solvers. *Computer Physics Communications*, 150(3):247–266, 2003.
- [24] Francis Filbet and Eric Sonnendrücker. Numerical methods for the Vlasov equation. In *Numerical Mathematics and Advanced Applications*, pages 459–468, Milano, 2003. Springer Milan.
- [25] Francis Filbet, Eric Sonnendrücker, and Pierre Bertrand. Conservative numerical schemes for the Vlasov equation. *Journal of Computational Physics*, 172(1):166–187, 2001.
- [26] Francis Filbet, Tao Xiong, and Eric Sonnendrücker. On the Vlasov–Maxwell system with a strong magnetic field. *SIAM Journal on Applied Mathematics*, 78(2):1030–1055, 2018.
- [27] Keshab Ganguly and H. D. Victory, Jr. On the convergence of particle methods for multidimensional Vlasov–Poisson systems. *SIAM Journal on Numerical Analysis*, 26(2):249–288, 1989.
- [28] Ernst Hairer, Christian Lubich, and Yanyan Shi. Large-stepsize integrators for charged-particle dynamics over multiple time scales. *arXiv preprint arXiv:2101.10403*, 2021.
- [29] Ernst Hairer, Christian Lubich, and Gerhard Wanner. *Geometric Numerical Integration. Structure-Preserving Algorithms for Ordinary Differential Equations*. Springer Series in Computational Mathematics 31. Springer, Berlin, Heidelberg, 2006.

- [30] Yang He, Hong Qin, Yajuan Sun, Jianyuan Xiao, Ruili Zhang, and Jian Liu. Hamiltonian time integrators for Vlasov–Maxwell equations. *Physics of Plasmas*, 22(12):124503, 2015.
- [31] Yang He, Yajuan Sun, Hong Qin, and Jian Liu. Hamiltonian particle-in-cell methods for Vlasov–Maxwell equations. *Physics of Plasmas*, 23(9):092108, 2016.
- [32] Yang He, Yajuan Sun, Ruili Zhang, Yulei Wang, Jian Liu, and Hong Qin. High order volume-preserving algorithms for relativistic charged particles in general electromagnetic fields. *Physics of Plasmas*, 23(9):092109, 2016.
- [33] Yang He, Zhaoqi Zhou, Yajuan Sun, Jian Liu, and Hong Qin. Explicit K-symplectic algorithms for charged particle dynamics. *Physics Letters A*, 381(6):568–573, 2017.
- [34] R. W. Hockney and J. W. Eastwood. *Computer Simulation Using Particles*. Institute of Physics Publishing, Bristol, 1988.
- [35] Shi Jin. Efficient Asymptotic-Preserving (AP) schemes for some multiscale kinetic equations. *SIAM Journal on Scientific Computing*, 21(2):441–454, 1999.
- [36] Michael Kraus, Katharina Kormann, Philip J. Morrison, and Eric Sonnendrücker. GEMPIC: Geometric electromagnetic particle-in-cell methods. *Journal of Plasma Physics*, 83(4):905830401, 2017.
- [37] Richard H. Levy. Diocotron instability in a cylindrical geometry. *The Physics of Fluids*, 8(7):1288, 1965.
- [38] Yingzhe Li, Yang He, Yajuan Sun, Jitse Niesen, Hong Qin, and Jian Liu. Solving the Vlasov–Maxwell equations using Hamiltonian splitting. *Journal of Computational Physics*, 396:381–399, 2019.
- [39] J. L. Lions and G. Stampacchia. Variational inequalities. *Communications on Pure and Applied Mathematics*, 20(3):493–519, 1967.
- [40] Jerrold E. Marsden and Tudor S. Ratiu. *Introduction to Mechanics and Symmetry*. Texts in Applied Mathematics. Springer, New York, 1999.
- [41] Jerrold E. Marsden and Alan Weinstein. The Hamiltonian structure of the Maxwell–Vlasov equations. *Physica D: Nonlinear Phenomena*, 4(3):394–406, 1982.
- [42] Robert I. McLachlan and G. Reinout W. Quispel. Splitting methods. *Acta Numerica*, 11:341–434, 2002.
- [43] Michel Mehrenberger, Eric Violard, Olivier Hoenen, Martin Campos Pinto, and Eric Sonnendrücker. A parallel adaptive Vlasov solver based on hierarchical finite element interpolation. *Nuclear Instruments and Methods in Physics Research Section A: Accelerators, Spectrometers, Detectors and Associated Equipment*, 558(1):188–191, 2006.
- [44] P. J. Morrison. A general theory for gauge-free lifting. *Physics of Plasmas*, 20(1):012104, 2013.
- [45] Philip J. Morrison. The Maxwell–Vlasov equations as a continuous Hamiltonian system. *Physics Letters A*, 80(5):383–386, 1980.
- [46] Philip J. Morrison. Hamiltonian description of the ideal fluid. *Review of Modern Physics*, 70:467–521, Apr 1998.
- [47] Philip J. Morrison. Structure and structure-preserving algorithms for plasma physics. *Physics of Plasmas*, 24:055502, 2017.
- [48] Peter J. Olver. *Applications of Lie Groups to Differential Equations*. Graduate Texts in Mathematics. Springer, New York, 1986.
- [49] M. Perin, C. Chandre, P. J. Morrison, and E. Tassi. Hamiltonian fluid closures of the Vlasov–Ampère equations: From water-bags to n moment models. *Physics of Plasmas*, 22(9):092309, 2015.
- [50] Anthony J. Peurrung and Jack Fajans. Experimental dynamics of an annulus of vorticity in a pure electron plasma. *Physics of Fluids A: Fluid Dynamics*, 5(2):493–499, 1993.
- [51] Martin Campos Pinto, Katharina Kormann, and Eric Sonnendrücker. Variational Framework for Structure-Preserving Electromagnetic Particle-In-Cell Methods. *arXiv preprint arXiv:2101.09247*, 2021.
- [52] Hong Qin, Jian Liu, Jianyuan Xiao, Ruili Zhang, Yang He, Yulei Wang, Yajuan Sun, Joshua W. Burby, Leland Ellison, and Yao Zhou. Canonical symplectic particle-in-cell method for long-term large-scale simulations of the Vlasov–Maxwell equations. *Nuclear Fusion*, 56(1):014001, 2016.
- [53] P. A. Raviart. An analysis of particle methods. In Franco Brezzi, editor, *Numerical Methods in Fluid Dynamics*, pages 243–324, Berlin, Heidelberg, 1985. Springer Berlin Heidelberg.
- [54] Magdi Shoucri. *Numerical Simulation of the Bump-on-Tail Instability. Numerical Simulations-Applications, Examples and Theory*. IntechOpen, Rijeka, 2011.
- [55] Jonathan Squire, Hong Qin, and William M. Tang. Geometric integration of the Vlasov–Maxwell system with a variational particle-in-cell

- scheme. *Physics of Plasmas*, 19(08):084501, 2012.
- [56] Jianyuan Xiao, Hong Qin, and Jian Liu. Structure-preserving geometric particle-in-cell methods for Vlasov–Maxwell systems. *Plasma Science and Technology*, 20(11):110501, sep 2018.
- [57] Jianyuan Xiao, Hong Qin, Jian Liu, Yang He, Ruili Zhang, and Yajuan Sun. Explicit high-order non-canonical symplectic particle-in-cell algorithms for Vlasov–Maxwell systems. *Physics of Plasmas*, 22:112504, 2015.
- [58] Haruo Yoshida. Construction of higher order symplectic integrators. *Physics Letters A*, 150(5):262–268, 1990.
- [59] Yuhua Zhu and Shi Jin. The Vlasov–Poisson–Fokker–Planck system with uncertainty and a one-dimensional asymptotic preserving method. *Multiscale Modeling & Simulation*, 15(4):1502–1529, 2017.